ISSN 1075-7015, Geology of Ore Deposits, 2006, Vol. 48, No. 5, pp. 335–356. © Pleiades Publishing, Inc., 2006.
Original Russian Text © N.P. Laverov, S.V. Yudintsev, S.V. Stefanovsky, B.I. Omel'yanenko, B.S. Nikonov, 2006, published in Geologiya Rudnykh Mestorozhdenii, 2006, Vol. 48, No. 5, pp. 387–409.

Muratаite As a Universal Matrix for Immobilization of Actinides

N. P. Laverov[a], S. V. Yudintsev[a], S. V. Stefanovsky[b], B. I. Omel'yanenko[a], and B. S. Nikonov[a]

[a]*Institute of Geology of Ore Deposits, Petrography, Mineralogy, and Geochemistry, Russian Academy of Sciences, Staromonetnyi per. 35, Moscow, 119017 Russia*

[b]*State Unitary Enterprise Joint Ecological–Technological and Research Center for Neutralization of Radioactive Wastes and Environmental Protection (MosNPO Radon), Sed'moi Rostovskii per. 2/14, Moscow, 119121 Russia*

Received June 16, 2006

Abstract—A new variety of matrices based on synthetic phases whose structure is close to that of murataite (a natural mineral) is proposed for immobilization of nuclear wastes. Murataite is Na, Ca, REE, Zn, and Nb titanate with a structure derived from the fluorite lattice. This very rare mineral was found in alkali pegmatites from Colorado in the United States and the Baikal region in Russia. The synthetic murataite-like phases contain manganese instead of zinc, as well as actinides and zirconium instead of sodium, calcium, and niobium. Varieties with threefold, as in the mineral, and five-, seven-, and eightfold repetition of the lattice relative to the fluorite cell have been established. Correspondingly, the structural varieties M3, M5, M7, and M8 are recognized among the synthetic murataites. A decrease in the contents of actinides, rare earth elements, and zirconium occurs in the series M7–M5–M8–M3, along with enrichment in Ti, Al, Fe, and Ga. Murataite-based ceramics are characterized by high chemical and radiation stability. The rate of U, Th, and Pu leaching with water at 90°C in static and dynamic tests is 10^{-6}–10^{-5} g/m^2 per day. These values are lower than the leaching rate of other actinide confinement matrices, for example, zirconolite- or pyrochlore-based. Murataite is close to other titanates in its radiation resistance. At 25°C, amorphization of its lattice is provided by a radiation dose of 2×10^{18} α decays/g, or 0.2 displacements/atom. Murataite-based matrices are synthesized within a few hours by cold compacting combined with sintering at 1300°C or by melting at 1500–1600°C and subsequent crystallization. The melting technology, including induction smelters with a cold crucible, makes it possible to produce samples with zonal murataite grains. The inner zone of such grains is composed of structural variety M5 or M7; the intermediate zone, of M8; and the outer zone, of M3. The contents of actinides, zirconium, and rare earth elements reach a maximum in the inner zone and drop to a minimum in the outer zone, while the amounts of nonradioactive elements—Ti, Al, Fe, and Ga—vary conversely. The U, Th, and Pu contents in the inner and outer zones differ by three to five times. Such a distribution precludes removal of actinides by interaction of the matrix with solution after its underground disposal. Individual actinides (Np, Pu, Am); the actinide–zirconium–rare earth fraction of high-level radioactive wastes (HLW); Am–Ga residues of weapons plutonium reprocessing with its conversion into U–Pu mixed oxide (MOX) fuel; and other sorts of HLW enriched in actinides, REE, and products of corrosion (Mn, Fe, Al, Zr) can be incorporated into a murataite-based matrix. As much as 350 kg of HLW components can be included in 1 t of such a ceramic. An actinide matrix that is composed of titanates with a pyrochlore structure is its nearest analogue. The advantage of murataite in comparison with pyrochlore consists in its universal character; i.e., a murataite-based matrix can be used for utilization of a wider range of actinide-bearing highly radioactive wastes.

DOI: 10.1134/S1075701506050011

INTRODUCTION

The production of fissile materials for military purposes and reprocessing of spent nuclear fuel (SNF) of civilian nuclear power plants has resulted in the accumulation of great amounts of radioactive wastes. For example, the recovery of U and Pu from 1 t of SNF from a VVER-440 reactor yields 13, 78, and 1875 m^3 of liquid high-, intermediate-, and low-level radioactive wastes (HLW, ILW, and LLW), respectively (Kopyrin et al., 2006). HLW, which contain more than 90% of the total radioactivity of wastes, are the most environmentally hazardous. HLW include actinides, products of their fission, corrosion elements, etc. More than 30000 m^3 of liquid HLW with activity above 350 MCi have been accumulated in Russia as a result of reprocessing of SNF on the territory of the Mayak Production Association (PO Mayak) in the southern Urals (*End Points*…, 2003). The long-lived actinides with half-lives from hundreds of years (americium) to tens of thousands or millions of years (plutonium, neptunium) are the most hazardous elements. Therefore, the safety of underground storage facilities is, to a great extent, determined by their ability to isolate actinides for a long time span. The confinement matrix is most important in ensuring this condition.

In compliance with IAEA requirements, liquid HLW must be solidified by means of their incorporation into stable confinement matrices. The matrix

Corresponding author: S.V. Yudintsev. E-mail: syud@igem.ru

Table 1. Compositions of natural (1, 2) and synthetic (3) murataite, wt %

No.	Na_2O	Al_2O_3	CaO	TiO_2	MnO	FeO	ZnO	Y_2O_3	Ln_2O_3	ZrO_2	Nb_2O_5	UO_2	F
1	5.8	n.d.	0.9	37.9	0.6	4.4	12.5	12.1	9.7	n.d.	10.0	n.a.	6.5
2	5.9	″	6.7	48.2	n.d.	2.3	16.2	20.5	0.7	″	n.d.	″	n.d.
3	0.7	9.3	7.8	32.1	7.8	23.4	n.d.	n.d.	1.0	13.2	″	3.3	″

Note: Ln_2O_3 is the REE, mainly HREE, sum. (1) After Adams et al. (1974); (2) after Portnov et al. (1981); (3) after Morgan and Ryerson (1982). Here and hereafter: n.d. denotes not detected; n.a. denotes not analyzed.

serves as one of the main elements in the multibarrier system of protection of the biosphere from radionuclides. High strength, homogeneity, thermal conductance, capacity, and radiation and chemical stability, as well as an economically efficient technology of production, are the key requirements for such materials (*GOST* (State Standard) *R 50926-96*, 1996). The search for optimal HLW matrices has been continuing for about 50 years, largely in regard to immobilization of liquid waste left behind SNF reprocessing. The industrial immobilization of HLW in Na–Al–P and Na–B–Si glass matrices has been carried out for decades. These glasses are not able to ensure the long-term isolation of radionuclides. Therefore, the elaboration of new types of durable HLW matrices is an important problem.

We participated in obtaining and studying polyphase Synroc-type matrices (Stefanovsky et al., 1996) and zirconolite-, pyrochlore-, and ferrigarnet-based ceramics (Laverov et al., 1996; Stefanovsky et al., 1997; Laverov et al., 2001; Yudintsev, 2003), as well as in elaboration of general problems of mineralogy and geochemistry of HLW-confining matrices (Laverov et al., 1997, 1998b, 2002). It was shown that most of the known titanate (pyrochlore, perovskite)-, phosphate (monazite)-, and silicate (zircon)-based matrices are intended for immobilization of a relatively narrow range of components (actinides, occasionally in combination with REE). We have attempted to work out a universal matrix for actinide HLW that would include other constituents of wastes, products of corrosion above all else. Matrices that contain 80–95% synthetic murataite are proposed as promising materials (Laverov et al., 1998c, 1999; Stefanovsky et al., 2001; Yudintsev et al., 2001). A large amount of new data on the properties of murataite-based matrices has been obtained recently, and this paper is the most comprehensive summary of the research carried out.

GENERAL INFORMATION ABOUT MURATAITE

Natural murataite is a very rare mineral that has been found in alkali pegmatite from El Paso County, Colorado, in the United States (Adams et al., 1974) and later from the Baikal region in Russia (Portnov et al., 1981). This mineral is an HREE, Zn, Na, and Fe titanate (Table 1). Murataite from Colorado is distinguished by high Nb and F contents, while that from the Baikal region is devoid of these elements but contains calcium. Some differences have been established in REE. While total REE contents are similar (21–22 wt %), murataite from Colorado contains Y and HREE in equal amounts, whereas Y is sharply prevalent in the mineral from the Baikal region. The structural study of the sample from Colorado (Ercit and Hawthorne, 1995) confirmed the cubic lattice of the mineral (space group $F\bar{4}3m$, a = 14.89 Å, Z = 4) and allowed an idealized formula $A_6B_{12}C_4TX_{40-x}$ (A = Y, Na; B = Ti; C = Fe; T = Zn; X = O, F) to be proposed. Four cation sites are distinguished: (A) distorted cube, (B) octahedron, (C) pentatope, and (T) tetrahedron. No radioactive elements are contained in natural murataite, and, therefore, in contrast to zirconolite, pyrochlore, monazite, and other U- and Th-bearing minerals, synthetic analogues of murataite were not considered a matrix for actinides previously.

A synthetic murataite-like phase was found for the first time in a titanate ceramic with HLW imitators produced at the Savannah River Plant in the United States (Morgan and Ryerson, 1982). A similarity to natural murataite was suggested from XRD data. It was pointed out that the structure of this phase may be expressed via an oxide motif of fluorite type with a threefold unit cell. According to microprobe results, the formula was written as $[(Ca,Mn)_2Zr(Fe,Al)_4Ti_3O_{16}]$. In contrast to the natural mineral, the synthetic phase is devoid of Zn but contains Mn, Zr, Al, and U (Table 1). The U content turned out to be four times lower than in zirconolite from the same sample. Therefore, at that time, murataite did not attract interest as a possible actinide matrix.

The study of murataite was stimulated by the discovery of this mineral in Synroc matrix with imitators of wastes from PO Mayak (Laverov et al., 1997). Five volume percent of this mineral accumulated about 40% of the total uranium regardless of the occurrence in the sample of such high-capacity with respect to actinides phases as zirconolite and perovskite (Fig. 1). These data initiated the purposeful investigation of synthetic HLW matrices with murataite as the dominant phase (Laverov et al., 1998b, 1998c, 1999; Stefanovsky et al., 2001).

Murataite varieties with three- (as in natural M3 murataite), five-, eight-, and very rare sevenfold repetition of the lattice with respect to the fluorite-type cell have been detected, and, correspondingly, the varieties

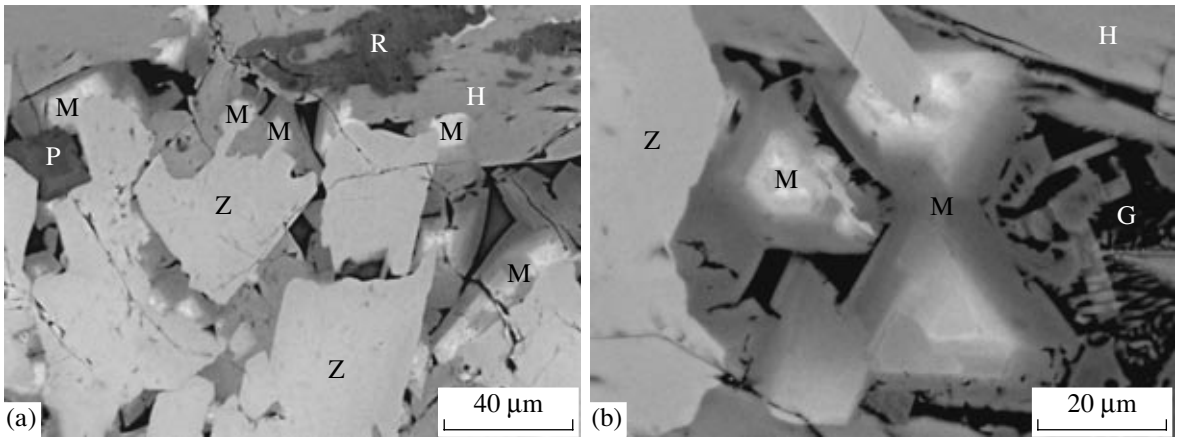

Fig. 1. The Synroc matrix with 20% HLW imitators from PO Mayak, SEM image. (M) Zonal murataite grain, (Z) zirconolite, (H) hollandite, (R) rutile, (P) perovskite, (G) glass.

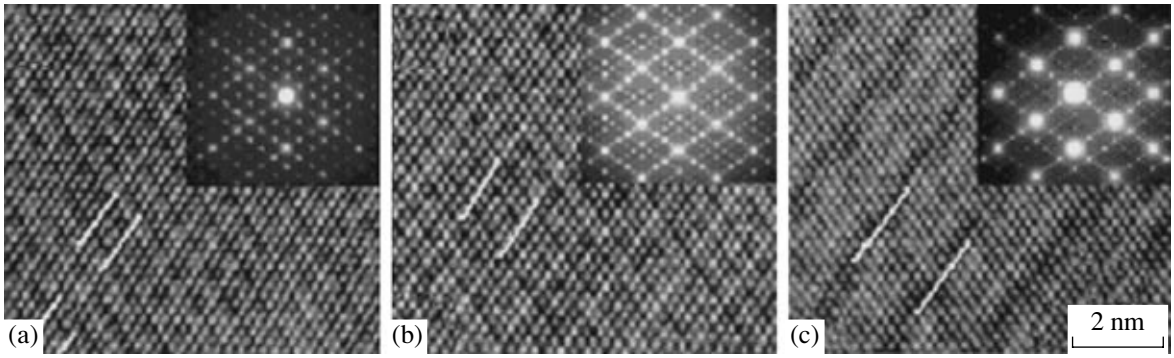

Fig. 2. HRTEM images of murataite phases: (a) M3, (b) M5, and (c) M8. Lines denote repetition of layer position in the structure. The insets show electron diffraction patterns from plane (110)* in murataites M3, M5, and M8.

M3, M5, M8 (Fig. 2), and M7 of synthetic murataite are recognized. It has been shown that Mn is necessary for their formation along with Ti and large actinide and REE cations (Laverov et al., 1997). Attempts to produce Zn-murataite from a charge close in composition to this mineral failed, most likely, because of a difference between the run parameters and the formation conditions of murataite in nature. It was established that actinide murataite-based ceramics are highly resistant to water and are not inferior to matrices based on pyrochlore-type titanate in radiation resistance (Laverov et al., 2003).

These specific features stimulated further detailed investigations of murataite as an actinide matrix. The studies were aimed at examining the actinide and REE isomorphism in murataite in order to find the optimal matrix composition, estimate the stability of phases under irradiation, and unravel their behavior in solutions. To choose efficient methods of murataite synthesis, ceramic samples produced with different methods from a similar charge were compared. The most important results are discussed below.

RESEARCH METHODS

The samples were obtained by cold compaction combined with sintering at 1100–1300°C, by melting at 1500°C in an electric furnace, or by induction melting in a cold crucible (IMCC) at 1600°C. The synthesis was carried out at the Mendeleev University of Chemical Technology of Russia and MosNPO Radon. Samples with transuranic actinides (Np, Pu, Am) were prepared at the Institute of Geochemistry and Analytical Chemistry (GEOKhI) of the Russian Academy of Sciences and at the Research Institute of Atomic Reactors (RIAR) (Cm). An oxide charge was powdered and homogenized in an LIV-0.5E linear induction rotator or in an AGO-2U planetary mill, then pressed into pellets 8–10 mm in diameter and 2–4 mm high at room temperature and afterward heated to 1100–1500°C. The runs were performed in alundum crucibles at 1100–1300°C and in platinum or glass-carbon ampoules at a higher temperature. After the runs, the samples were studied with XRD, SEM/EDS, and TEM, high-resolution TEM (HRTEM) included. To determine the radiation stability, the samples were irradiated with a 1 MeV Kr^{2+} ion beam or by doping with 2 wt % ^{244}Cm. The

study was carried out in cooperation with specialists from the University of Michigan (United States) and RIAR. The matrix stability in water was tested in the static and dynamic regimes at 95°C at the Laboratory of Radiochemistry of GEOKhI RAS and at MosNPO Radon.

ACTINIDE AND REE ISOMORPHISM IN MURATAITE PHASES

To study the incorporation of chemical elements into murataite, a series of samples was synthesized. Most investigations were performed with a basic charge composition (wt %) 55 TiO_2, 10 MnO, 10 CaO, 5 Al_2O_3, 5 Fe_2O_3, 5 ZrO_2, and 10 HLW components. Actinide oxides (UO_2, ThO_2, NpO_2, PuO_2) and REE oxides (La_2O_3, CeO_2, Pr_6O_{11}, Nd_2O_3, Sm_2O_3, Eu_2O_3, Gd_2O_3, Tb_2O_3, Dy_2O_3, Y_2O_3) or mixtures of them corresponding to the compositions of actinide or actinide–REE fractions served as imitators of wastes. The aforementioned proportion of components allows a maximum amount of murataite to be obtained (Laverov et al., 1999). In addition to murataite, the samples contained other titanate phases: structural analogues of minerals from the rutile group (space group $P4_2/mnm$, formula [Ti,Zr]O_2), crichtonite (*R3*, [Ca,REE,An][Ti, Zr,Fe,Al]$_{21}O_{38}$), perovskite (*Pnma*, [Ca,REE,An]TiO_3), ilmenite–pyrophanite (*R-3*, [Mn,Fe]TiO_3), and pyrochlore (*Fd3m*, [Ca,REE,An]$_2$[Ti,Zr]$_2O_7$). For simplicity, these synthetic phases are further referred to in the same way as their natural analogues.

The maximum amount of murataite is contained in two-phase ceramics where rutile or crichtonite occurs along with murataite. Attempts to synthesize single-phase murataite samples, including runs with a charge containing the same percentage of titanium as in murataite, failed. In this case, a mineral assemblage composed of phases either with a lower Ti content than in murataite, e.g., pyrochlore and perovskite, or with a higher Ti content (crichtonite and rutile) was formed. In general, it was established that a charge of optimal composition must contain an excess of titanium, which is fixed in rutile or crichtonite after murataite crystallization.

Several murataite varieties, commonly M3, M5, and M8, were revealed in most samples. The phase with sevenfold repetition of the lattice relative to the fluorite cell (M7) is extremely rare. The general term *murataite* is applied to all these varieties; the specific murataite variety is indicated when necessary and when TEM or HRTEM data are available.

REE-Bearing Matrices

As follows from the XRD data, murataite is predominant in all REE-bearing samples except La-bearing ones, where perovskite and murataite occur in commensurable amounts (Fig. 3). Titanates with crichtonite, pyrophanite, rutile, and less frequently pyrochlore structures are detected in almost all samples. The *d* spacings for the main reflections of murataite are within the ranges 2.86–2.79, 2.47–2.43, 1.75–1.72, and 1.50–1.42 Å; several closely located or partially overlapped reflections are detected in each of these ranges. This is apparently caused by occurrence of several murataite modifications, as is corroborated in some cases by TEM and HRTEM observations. Murataite and perovskite are the main REE concentrators in the ceramics (Table 2); in the samples containing LREE (from La to Sm), some elements are incorporated into crichtonite. Perovskite is a typical phase in LREE-bearing ceramics; the greatest amounts of this mineral were detected in the sample that contained La (Figs. 3, 4). Perovskite contains largely LREE and MREE, whereas HREE fractionate into murataite phases. This is especially characteristic of the elements from Tb to Yb and of Y. While the Y partition coefficient between murataite M5 and perovskite is ~7, the partition coefficient decreases to 0.3 for Nd and 0.1 for still larger La (Table 2). A prevalence of HREE and Y is also typical of natural murataite. It is noteworthy that the Y-bearing sample is represented by the greatest number (four) of murataite varieties, including the very rare variety M7 (Table 2, Fig. 4).

The greatest amount of analytical data were obtained for the Gd-bearing sample, where several murataite phases, crichtonite, and pyrophanite were identified; the varieties M3, M5, and M8 occur in this sample. SEM images demonstrate the zonal structure of murataite grains, with phase M5 in the core and phase M8 at the margins. These grains are incorporated into a matrix composed of phase M3. Phase M8 is predominant, while murataites M5 and M3 occur in approximately equal quantities (Fig. 4). The Gd content is three times higher in M5 than in M3; the difference in Zr content is still higher. The Al and Fe contents decrease by three to five times on passing from M5 to M3, while the Ti content drops by 10%.

Murataite-Based Matrices with Actinides

In the samples with actinides, murataite prevails over crichtonite, rutile, perovskite, and pyrophanite (Figs. 5–7). The overwhelming majority of actinides occur in murataite. Their concentration in crichtonite and pyrophanite is extremely low, often below the detection limit (Table 3). The octahedral murataite crystals reveal a distinct zoning (Fig. 6). The inner zone is composed of variety M5; the intermediate zone, of M8; and the outer zone, of M3 (Figs. 7, 8), as was observed in the REE-bearing ceramics. As can be seen from the data obtained with SEM/EDS (Table 3, Fig. 9), the compositional variation of grains is similar to the systematic pattern revealed in the REE-bearing ceramics. As variety M5 gives way to variety M3 in the outward direction, the contents of actinides and Zr decrease, whereas the Ti, Fe, and Al contents increase. This trend is pointed out with respect to all actinides (U, Th, Pu, Np), but with a different intensity.

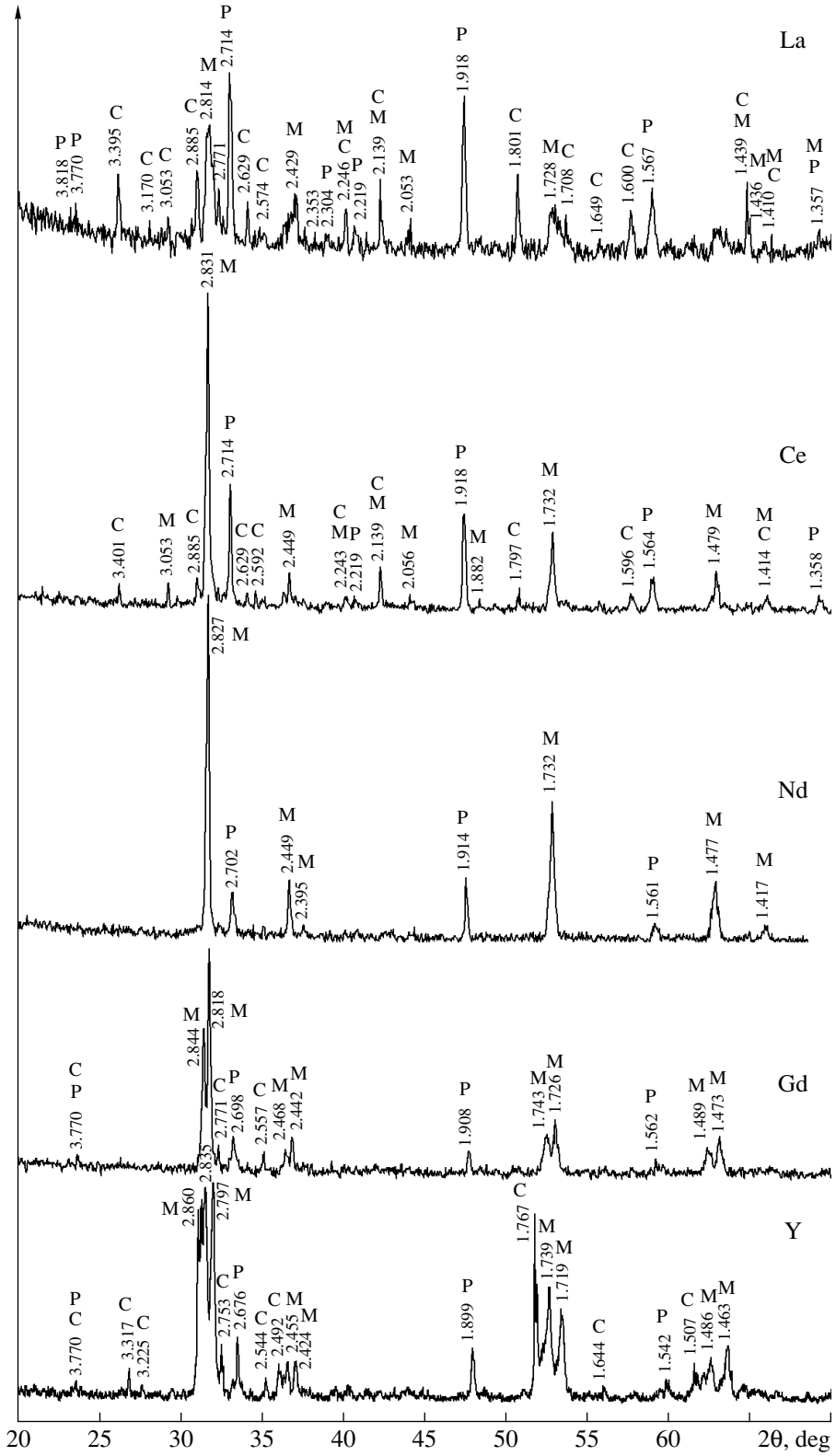

Fig. 3. X-ray patterns of REE-bearing ceramics. M, murataite (all varieties, unspecified); C, crichtonite; P, perovskite.

Table 2. Phase compositions in REE-bearing murataite-based ceramics, wt %

Oxide	La-bearing sample					Nd-bearing sample				Gd-bearing sample					Y-bearing sample						
	M5	M8	P	C	T	M5	M8	P	C	M5	M8	M3	C	T	M7	M5	M8	M3	P	C	T
Al_2O_3	3.8	8.3	1.4	5.3	n.d.	4.5	5.3	1.2	4.7	1.6	3.7	7.3	4.5	0.6	0.7	2.2	3.6	6.4	1.8	4.3	0.4
CaO	6.7	6.6	22.5	2.7	0.3	8.3	8.5	23.6	3.8	7.6	9.3	9.4	5.0	0.6	5.4	6.1	7.7	9.3	27.6	8.3	n.d.
TiO_2	47.9	50.1	48.3	65.0	51.7	52.9	55.3	46.3	70.3	46.4	53.5	56.7	72.9	52.7	47.0	51.2	54.7	58.6	58.6	67.3	53.8
MnO	13.0	15.0	1.5	9.2	29.0	10.5	10.3	1.8	8.3	6.5	8.4	11.1	7.2	25.2	4.4	5.5	8.3	10.7	4.9	7.7	26.2
Fe_2O_3	4.9	7.0	0.6	6.1	18.1*	4.3	6.2	n.d.	6.2	2.0	2.6	6.6	6.7	20.3*	1.2	2.0	2.9	5.4	2.7	7.2	19.1*
ZrO_2	23.2	8.4	n.d.	4.6	0.6	8.7	4.0	n.d.	2.1	16.9	8.4	3.3	0.8	n.d.	13.6	11.3	7.4	3.4	n.d.	1.2	n.d.
La_2O_3	1.9	3.1	25.1	6.5	n.d.	–	–	–	–	–	–	–	–	–	–	–	–	–	–	–	–
Nd_2O_3	–	–	–	–	–	8.4	8.7	24.9	4.5	–	–	–	–	–	–	–	–	–	–	–	–
Gd_2O_3	–	–	–	–	–	–	–	–	–	18.3	12.9	5.4	n.d.	n.d.	–	–	–	–	–	–	–
Y_2O_3	–	–	–	–	–	–	–	–	–	–	–	–	–	–	28.8	20.1	14.5	7.4	2.8	2.4	n.d.
Total	101.4	98.5	99.4	99.4	99.7	97.6	98.3	97.8	99.9	99.3	98.8	99.8	97.1	99.4	101.1	98.4	99.1	101.2	98.4	98.4	99.5

Note: Here and in Tables 3 and 5–8, M3, M5, M7, and M8 are murataites with three-, five-, seven-, and eightfold cells; P is perovskite; C, crichtonite; and T, pyrophanite.
* FeO is total Fe in the form of FeO. The dash indicates that an element was not introduced into a charge.

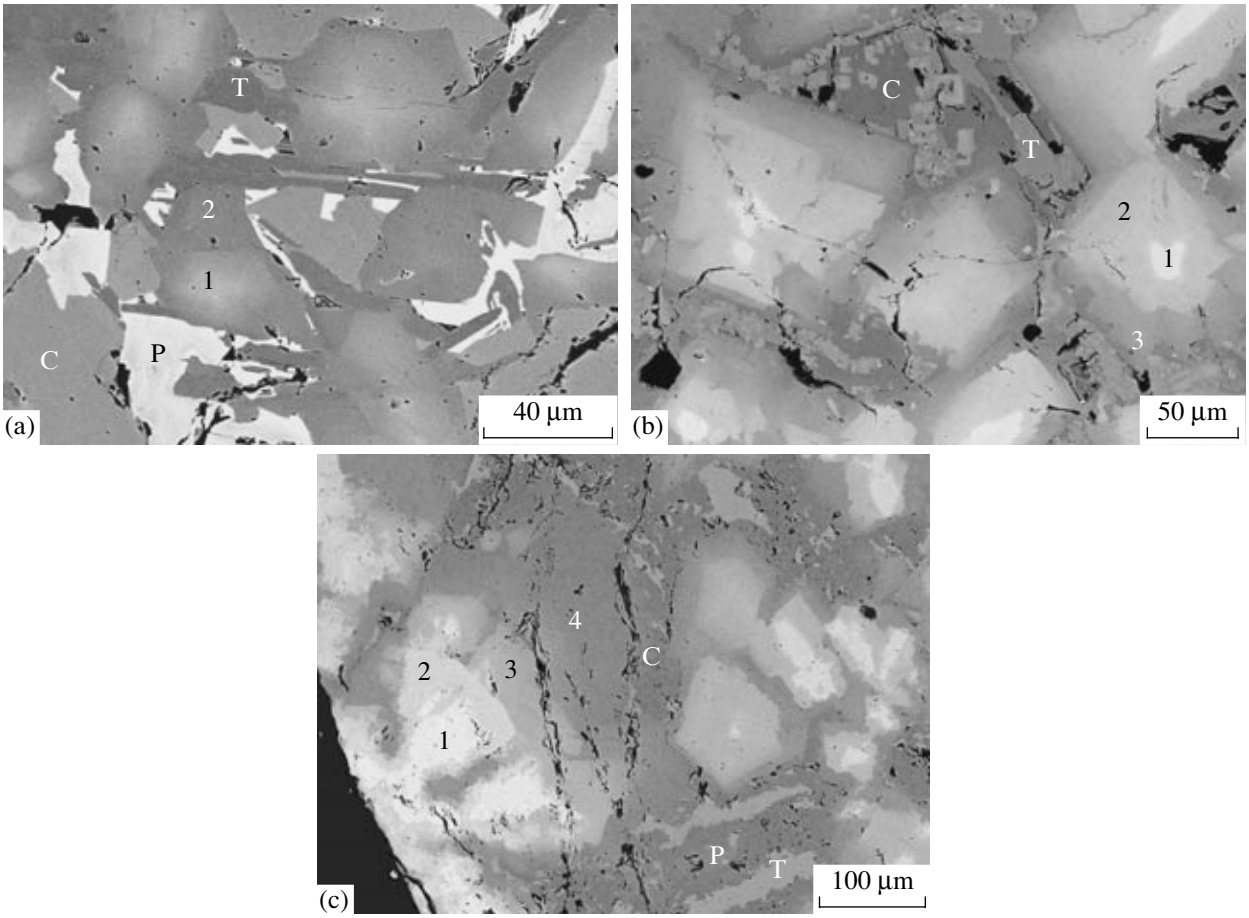

Fig. 4. SEM images of (a) La-, (b) Gd-, and (c) Y-bearing ceramics. (a, b) (1) M5, (2) M8, (3) M3; (c) (1) M7, (2) M5, (3) M8, (4) M3; C is crichtonite; P, perovskite; and T, pyrophanite.

Murataite Ceramics with Imitators of Actinide–REE Fractions of HLW

Three samples were studied (Table 4). U and Ce were introduced into the first sample (A). The other two ceramics were produced from a mixture that mimics the actinide–REE fraction of HLW. Sample B fits this fraction to the greatest extent. The conclusions on the behavior Am_2O_3 and Cm_2O_3 are based on the distribution of REE (Nd and Sm, above all else), which are regarded as imitators of trivalent actinides.

According to the XRD and SEM/EDS results (Figs. 10, 11), sample A is composed of 90% murataite phases; crichtonite and perovskite were detected as admixtures. The SEM images demonstrate the zoning of murataite grains typical of this kind of ceramics. The inner zone is enriched in U and Zr. The contents of these elements diminish toward the grain margins, while the Ti, Al, and Fe contents decrease in the same direction. By analogy with the samples bearing lanthanides and actinides, the zones distinct in color and composition may be referred to M5 (the core), M8 (the intermediate zones), and M3 (the marginal zones).

Murataite is the main concentrator of uranium, whereas the U contents in crichtonite and perovskite are below the detection limit. The LREE and MREE from La to Nd fractionate into perovskite, and the contrast in REE distribution between different phases diminishes as the atomic weight of an element increases (Table 5). The inverse pattern is typical of Sm (sample B): this element is mainly incorporated into murataite. A small amount of REE, largely LREE and MREE, is contained in crichtonite. Thus, while the LREE and MREE, with large ionic radii, are accumulated in perovskite and crichtonite, the HREE, with small ionic radii, are distributed in favor of murataite. This indicates that the compositions of synthetic and natural murataites are close to each other: both are enriched in HREE. This feature emphasizes a certain similarity of these minerals with synthetic titanates that correspond to ($REE_2Ti_2O_7$) in composition. Only the phases of MREE and HREE have the cubic structure of pyrochlore, whereas LREE titanates (from La to Sm) have monoclinic symmetry of the crystalline lattice.

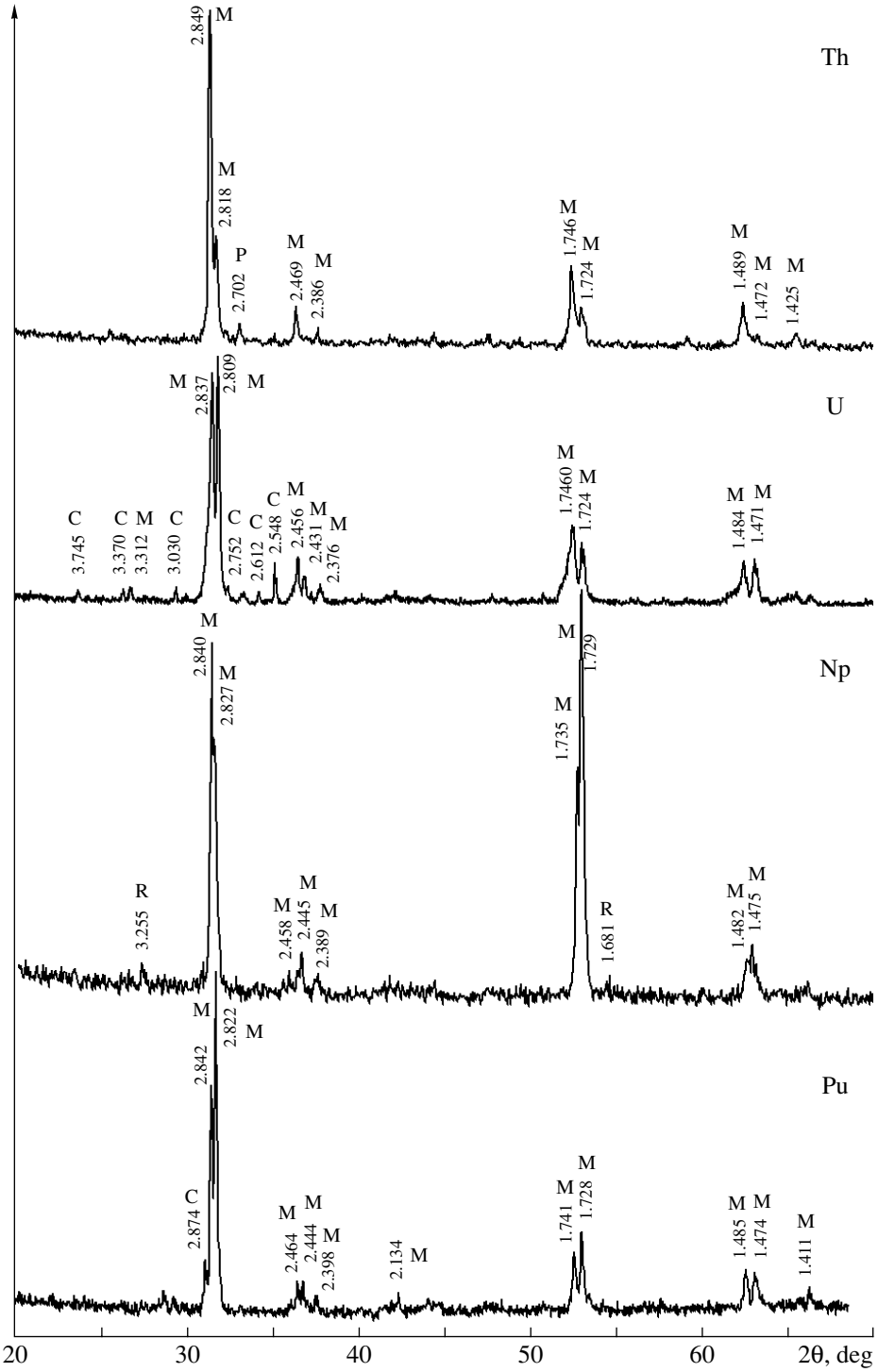

Fig. 5. X-ray patterns of actinide-bearing ceramics. M is murataite; P, perovskite; C, crichtonite; and R, rutile.

Ga-Bearing Murataite Ceramics

Taking into account the similar properties of several elements, one may suggest that synthesis of murataite ceramics of other compositions is also possible. For example, the similar dimensions of Al^{3+} and Fe^{3+}, on the one hand, and Ga^{3+}, on the other hand, allowed us to expect the possible formation of Ga ceramics. Hf may be incorporated into murataite instead of Zr, while Sn may replace Ti. Hafnium serves as a neutron absorber and prevents a fission chain reaction in actinide matrices. In this regard, the occurrence of Hf makes it possible to incorporate higher plutonium con-

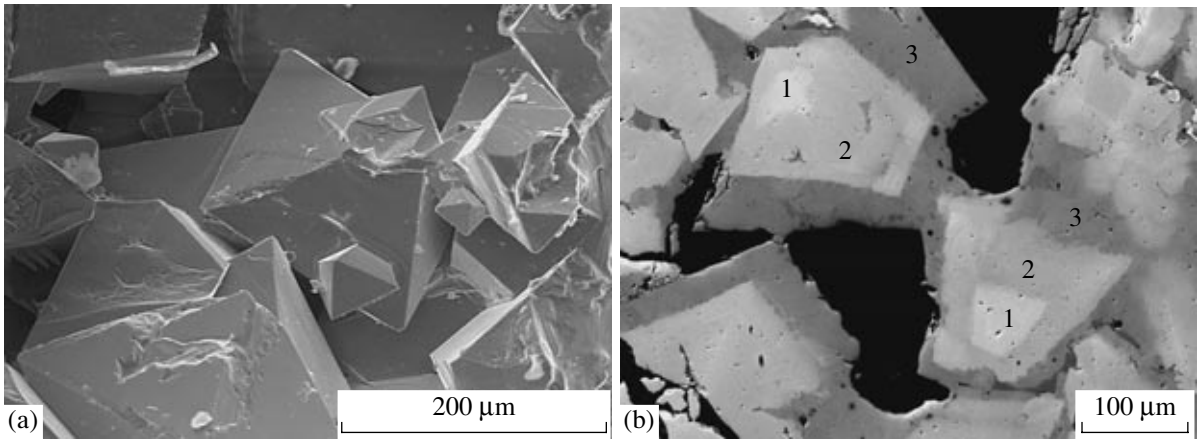

Fig. 6. SEM images of murataite-based ceramic containing 10 wt % ThO_2. (a) Intergrowth of murataite crystals; (b) structure of the same crystals in cross section. 1 is murataite M5; 2, murataite M8; and 3, murataite M3. See Table 4 for phase compositions.

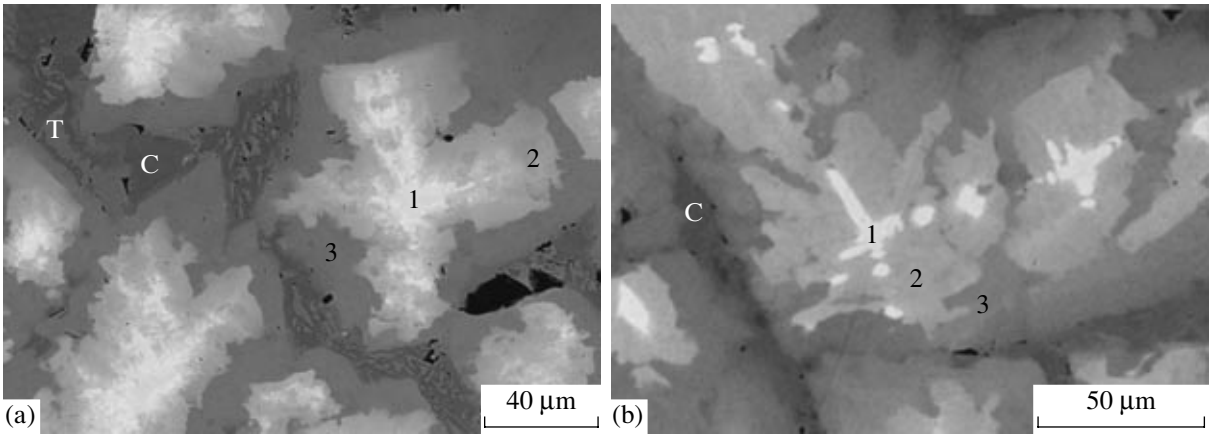

Fig. 7. SEM images of murataite-based ceramic containing (a) 10 wt % U and (b) 10 wt % Pu. 1 is murataite M5; 2, murataite M8; 3, murataite M3; C, crichtonite; and T, pyrophanite.

centrations into the murataite matrix. The incorporation of Ga into murataite is also a positive property of the matrix because Ga is a component of wastes that are formed by conversion of weapons plutonium into U–Pu mixed oxide (MOX) fuel.

In order to substantiate the possibility of Ga-murataite formation, a ceramic was synthesized from a charge into which gallium was introduced instead of the equivalent amount of aluminum. The composition of this ceramic was as follows (wt %): 55 TiO_2, 10 MnO,

Table 3. Phase compositions of ceramics with 10 wt % ThO_2 or 10 wt % UO_2

Oxide, wt %	Th-bearing sample					U-bearing sample				
	M5	M8	M3	P	C	M5	M8	M3	C	T
Al_2O_3	2.7	4.3	7.9	0.6	3.7	1.2	4.1	7.0	3.7	0.5
CaO	11.2	10.9	9.5	21.9	4.2	10.7	11.2	10.9	0.4	0.9
TiO_2	52.2	54.8	55.6	48.6	71.2	45.4	53.7	57.4	68.1	51.9
MnO	8.5	9.2	10.9	1.0	7.4	7.1	8.8	10.6	13.3	26.3
Fe_2O_3	3.0	3.6	7.2	0.6	8.4	2.1	3.5	5.7	16.1	19.7
ZrO_2	9.7	6.5	2.1	n.d.	1.3	12.2	7.0	3.1	n.d.	n.d.
$(Th/U)O_2$	12.6	10.9	5.1	24.1	2.7	21.5	11.3	4.6	″	″

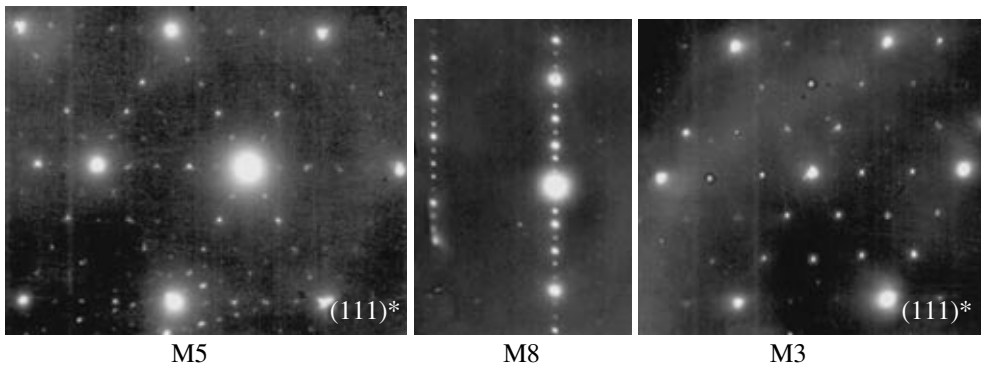

Fig. 8. Electron diffraction patterns of murataite (M5, M8, and M3) in a ceramic that contains 10 wt % PuO_2.

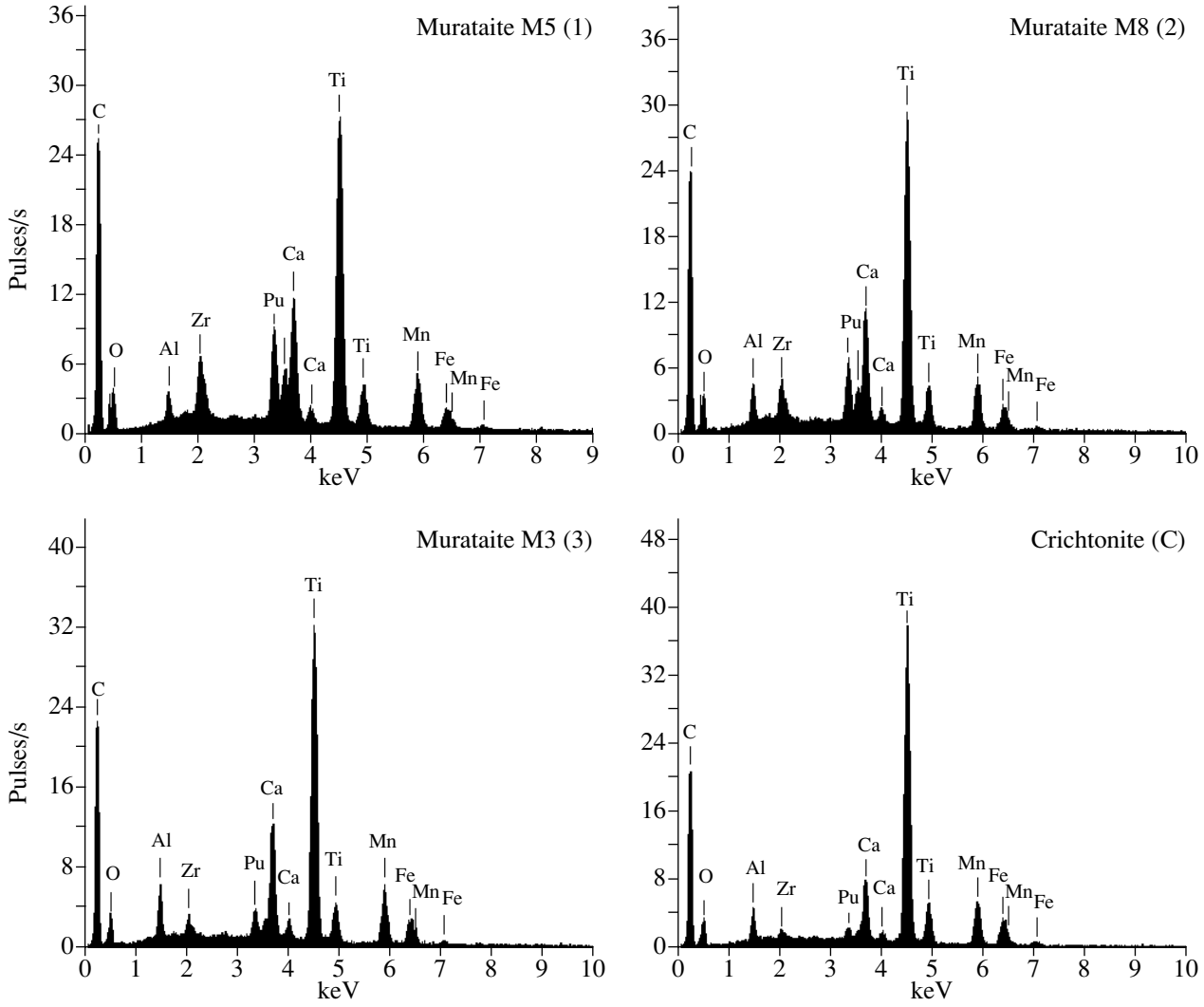

Fig. 9. The energy dispersive spectra of murataites M5, M8, and M3 (points 1–3) and crichtonite (point C) in the Pu-bearing sample. Point numbers correspond to the numerals in the SEM image in Fig. 7.

10 CaO, 5 Ga_2O_3, 5 Fe_2O_3, 5 ZrO_2, and 10 UO_2. The sample was obtained by compaction of the oxide mixture at 200 MPa and subsequent sintering at 1200°C for 5 h. According to the XRD data, the sample consisted of two murataite modifications, probably, M5 and M8, and crichtonite, rutile, and zirconolite admixtures. The

Table 4. Compositions of matrices with imitators of the actinide–REE fraction, wt %

Sample	Al_2O_3	CaO	TiO_2	MnO	Fe_2O_3	ZrO_2	La_2O_3	CeO_2	Pr_6O_{11}	Nd_2O_3	Sm_2O_3	UO_2
A	5.0	10.0	55.0	10.0	5.0	5.0	–	5.0	–	–	–	5.0
B	5.0	10.0	55.0	10.0	5.0	10.0	–	1.5	–	3.0	–	0.5
C	5.0	10.0	55.0	10.0	5.0	7.8	0.9	1.9	0.8	2.7	0.5	0.4

Note: The dash indicates that an element was not introduced into a charge.

compositions of these phases are given in Table 6. This sample differs from other ceramics in its high porosity and occurrence of rutile and zirconolite instead of pyrophanite.

VALENCE OF ELEMENTS IN MURATAITE

Some elements contained in murataite ceramics may occur with different degrees of oxidation depending on synthesis conditions. This is typical, first of all, of Fe and Mn and, to a lesser extent, of Ti. Furthermore, some samples contain REE, e.g., Ce or actinides (U, Np, Pu), which also have several degrees of oxidation. As was established in samples studied with Mössbauer spectroscopy (Urusov et al., 2002) and X-ray photoelectron spectroscopy (Maslakov et al., 2006), Fe and Mn occur in murataite as Fe^{3+} and Mn^{2+}, which is in agreement with results of X-ray absorption spectroscopy (Stefanovsky et al., 2006) testifying that more than 90% of Fe occurs in the trivalent state. Although Mn^{2+} is predominant (60–70%), a considerable percentage of Mn is in the form of Mn^{3+}. According to the data of X-ray photoelectron spectroscopy, actinides (U, Pu, Np) occur in murataite as tetravalent cations, while Ce is represented largely by Ce^{3+}.

EFFECT OF SYNTHESIS CONDITIONS ON SPECIFIC FEATURES OF MURATAITE-BASED CERAMICS

One of the requirements on actinide ceramics is the possibility of their economically efficient production.

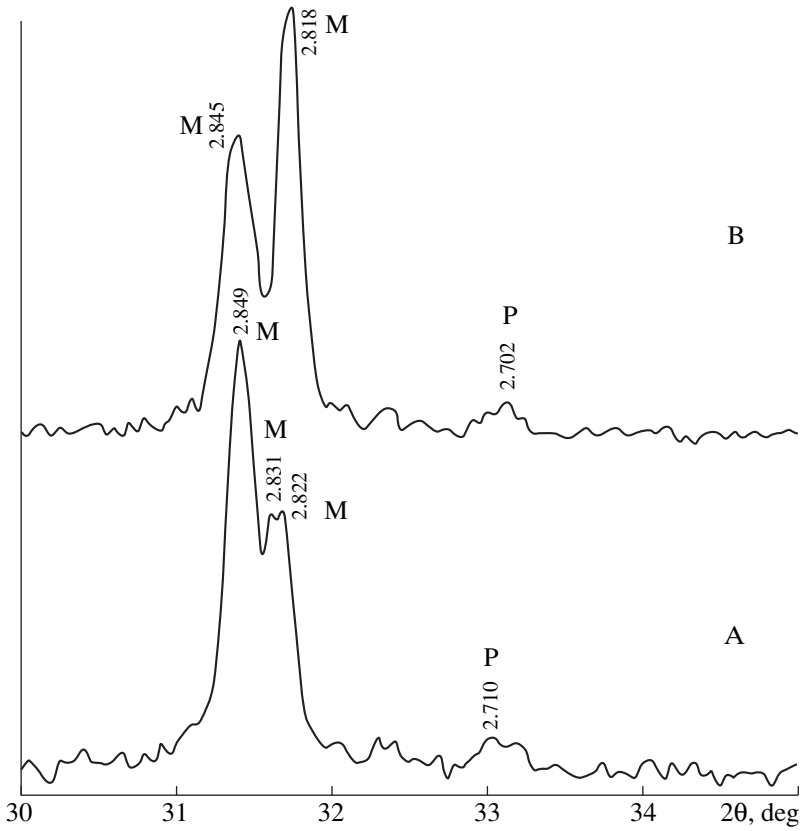

Fig. 10. Segments of X-ray patterns of samples A and B with imitators of the actinide–REE fraction in the region of intense murataite reflections. M is murataite phases; and P, perovskite.

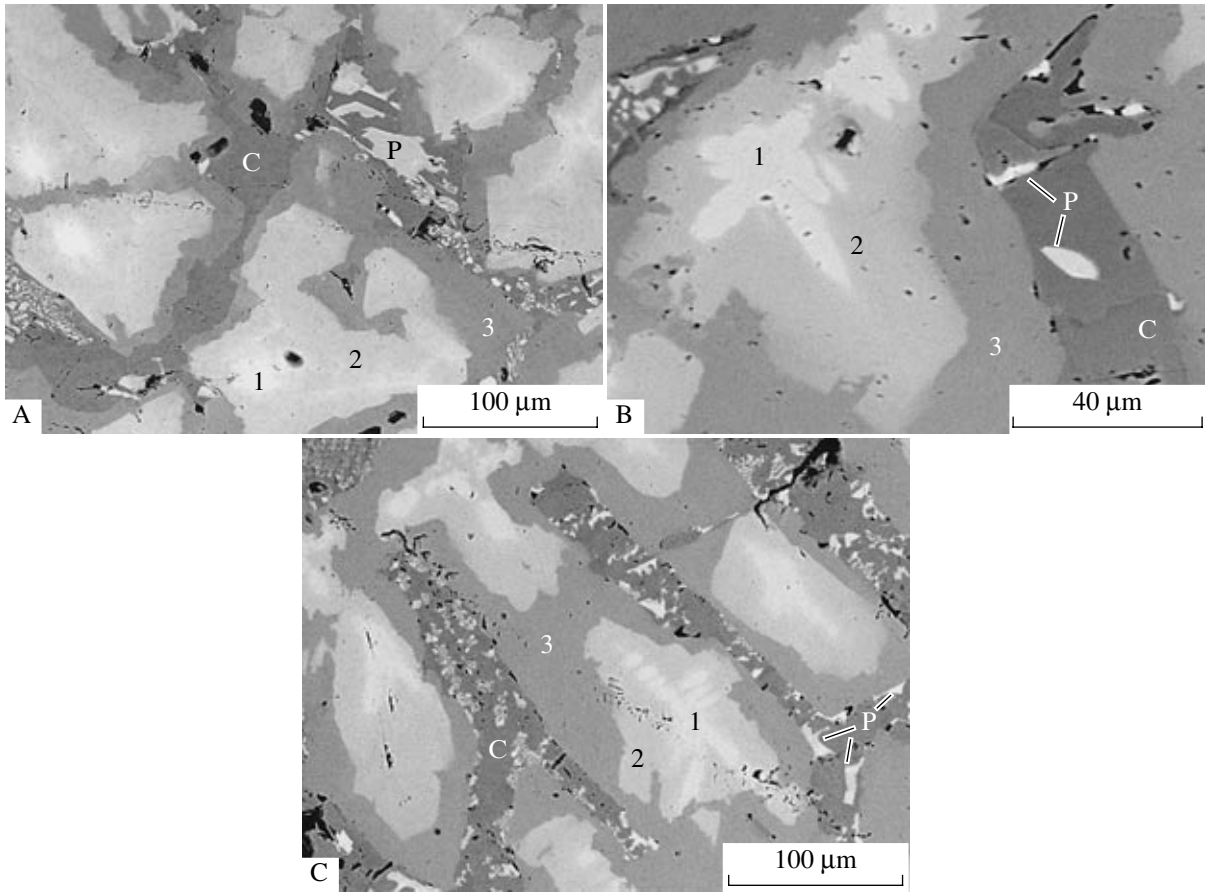

Fig. 11. SEM images of murataite-based ceramics with imitators of the actinide–REE fraction of HLW (samples A, B, and C). 1 is murataite M5; 2, murataite M8; 3, murataite M3; C, crichtonite; and P, perovskite.

The main methods of their manufacturing are solid-phase synthesis (hot or cold compaction + sintering) and melting–crystallization. Hot compaction is used in Australia for synthesis of Synroc (synthetic rock) materials (Ringwood, 1985) and zirconolite-based matrices (Vance et al., 1995). Under laboratory conditions, cold compaction and subsequent sintering at 1300–1400°C is commonly used for obtaining matrices for radioactive wastes (Laverov et al., 2001, 2002). Pyrochlore-based actinide matrices, including ones containing up to 12 wt % Pu, have been obtained by the same method in the United States (Strachan et al., 2005).

The high melting temperature (often above 1500°C) typical of crystalline matrices complicates their synthesis in common electric furnaces. The method of IMCC has been proposed for synthesis of refractory materials. Synroc ceramics (Stefanovsky et al., 1996), as well as zirconolite- and pyrochlore-based matrices (Stefanovsky et al., 1997, 2001), were previously obtained using this technology.

The specific features of ceramics produced with various methods are compared below. All of them were obtained from the same charge (wt %): 55 TiO_2, 10 MnO, 10 CaO, 5 Al_2O_3, 5 Fe_2O_3, 5 ZrO_2, and 10 UO_2. As was shown by the results of the preceding investigations, such a charge allows ceramics with the highest murataite content to be obtained. The mixtures were compacted and sintered for 4 h at 1100, 1300, and 1400°C or melted in an electric furnace at 1500°C or in an induction smelter with a cold crucible. The run parameters and phase compositions are summarized in Table 7. The study of these samples showed that temperature exerts substantial effects on their specific features.

The ceramic obtained as a result of cold compaction and sintering at 1100°C is characterized by incompleteness of phase formation reactions, as indicated by the following features:

(1) the occurrence of many other phases in addition to murataite; XRD study allowed identification of pyrochlore, perovskite, cubic U and Zr oxides, and rutile as well (Fig. 12);

(2) the retention of unreacted charge remains (ZrO_2, TiO_2, UO_2) in ceramics; and

(3) a significant volume of ceramic composed of aggregates of mineral grains with diffuse contours and less than 1 μm in size, which prevents their exact identification (Fig. 13).

Table 5. Phase compositions of samples with imitators of the actinide–REE fraction, wt %

Oxide	Sample A					Sample B					Sample C				
	M5	M8	M3	P	C	M5	M8	M3	P	C	M5	M8	M3	P	C
Al_2O_3	1.6	3.7	6.4	0.9	3.9	2.0	3.4	6.7	0.7	4.7	2.2	3.7	5.3	1.2	4.3
CaO	9.9	10.2	9.4	26.3	3.8	9.4	10.3	8.8	29.0	3.8	7.2	8.8	8.6	23.3	3.6
TiO_2	49.1	54.8	56.8	52.2	68.5	46.8	52.7	55.4	57.6	68.5	48.4	52.4	57.0	48.4	67.3
MnO	6.9	8.9	10.8	1.5	8.2	8.6	9.0	11.6	1.4	8.0	9.9	8.4	9.8	2.0	7.6
Fe_2O_3	2.4	3.9	5.3	0.9	7.7	2.5	3.0	4.7	n.d.	8.0	3.3	2.9	5.0	1.1	7.6
ZrO_2	13.4	8.0	3.4	n.d.	0.9	25.8	16.1	7.9	″	1.1	21.1	13.0	5.9	n.d.	1.5
La_2O_3	–	–	–	–	–	–	–	–	–	–	n.d.	n.d.	n.d.	3.0	1.1
Ce_2O_3	2.7	2.6	3.0	17.4	4.8	n.d.	n.d.	n.d.	4.5	n.d.	″	1.0	1.4	6.6	1.7
Pr_2O_3	–	–	–	–	–	–	–	–	–	–	″	0.7	0.9	2.4	1.1
Nd_2O_3	–	–	–	–	–	2.5	3.0	2.7	6.8	0.7	2.2	3.1	2.4	7.7	1.5
Sm_2O_3	–	–	–	–	–	–	–	–	–	–	0.8	1.1	0.6	0.4	n.d.
UO_2	10.6	5.9	2.2	n.d.	n.d.	1.0	0.7	0.3	n.d.	n.d.	3.1	2.6	2.0	n.d.	″
Total	96.6	98.0	97.3	99.2	97.8	98.6	98.2	98.1	100.0	94.8	98.2	97.7	98.9	96.1	97.3

Note: The dash indicates that an element was not introduced into a charge.

Table 6. Phase compositions of murataite-based ceramic containing 5 wt % Ga_2O_3

Oxide, wt %	M5	M8	C	R	Z
CaO	12.1	11.1	5.5	n.d.	12.0
TiO_2	38.8	47.0	62.9	94.4	38.7
MnO	4.7	10.2	12.8	0.7	4.4
Fe_2O_3	2.0	3.4	8.5	n.d.	1.8
Ga_2O_3	2.7	5.0	6.4	″	2.7
ZrO_2	22.9	11.0	1.4	1.7	30.5
UO_2	14.9	11.2	2.2	2.3	8.7
Total	98.1	98.9	99.7	99.1	98.8

Note: R, rutile and Z, zirconolite.

The specific features mentioned above indicate that the applied temperature and duration of sintering were not sufficient for obtaining a murataite-based ceramic with optimal properties.

The ceramic obtained as a result of cold compaction and sintering at 1300°C is characterized by completeness of phase formation reactions and the achievement of equilibrium in the system, as supported by several lines of evidence:

(1) the number of phases is limited, and murataite M8 dominates, followed by rutile and murataite M5 (Figs. 12, 13);

(2) relatively large mineral grains (5–20 μm), mainly composed of murataite M8, are prevalent;

(3) the grains of murataite M8 often contain tiny (from fractions of a micrometer to a few micrometers in size) inclusions of murataite M5 and rutile with clearly discernible contours;

(4) no unreacted charge remains are observable;

(5) structural relationships indicate that murataites M5 and M8 crystallize at the initial stage of synthesis and rutile is formed at the last stage.

In U, Al, and Fe contents, murataites M5 and M8 differ by 1.5–2.2 times; the differences in concentrations of other elements are much less (Table 8).

The ceramic obtained by melting in an electric furnace at 1500°C in a platinum crucible consists of three murataite varieties (M5, M8, and M3) and rutile (Figs. 12, 13). The murataite grains show zoning with a prevalence of M5 in the inner zone, M8 in the intermediate zone, and M3 in the outer zone (Fig. 13). The Ca, U, and Zr contents decrease from the crystal core outward, while the Mn, Ti, Fe, and Al contents increase in the same direction (Table 8). The boundaries between M8 and M3 are always rather distinct, while gradual transitions are established between M8 and M5. This indicates that equilibrium relationships between M8 and M3 are reached to a higher degree than between M8 and M5. The main body of the ceramic is composed of

Table 7. Run parameters and phase compositions of the samples obtained

Temperature of synthesis, °C/crucible type	Detected phases (listed in decreasing amounts)	Notes
1100/alundum crucible	Py or Z, M, O, R	No melting
1300/alundum crucible	M8, M5, R	
1400/alundum crucible	Corrosion of the alundum crucible caused by melting of the charge	
1500/platinum crucible	M5, M8, M3, R	Complete melting of the initial charge
~1600/IMCC	M5, M8, M3, R, C, G	

Note: Py is pyrochlore; Z, zirconolite; O, cubic oxide; R, rutile; C, crichtonite; and G, glass. IMCC, induction melting in a cold crucible.

Table 8. Phase compositions in samples (recalculated to 100%), wt %

Oxide	Electric furnace, 1300°C			Electric furnace, 1500°C				IMCC, ~1600°C			
	M5	M8	R	M5	M8	M3	R	M5 + M8	M3	R	C
Al_2O_3	1.3	2.9	0.2	2.1	4.5	7.1	0.5	3.8	9.5	0.5	6.7
CaO	13.2	11.8	0.3	13.8	12.6	11.4	0.2	11.2	9.4	0.4	4.5
TiO_2	50.7	51.1	92.6	48.6	52.7	52.5	90.3	51.6	53.0	92.5	66.5
MnO	7.3	9.2	0.6	7.3	9.6	10.8	0.5	8.8	11.2	0.3	9.9
Fe_2O_3	1.8	3.7	0.8	3.6	4.6	6.5	0.8	4.9	8.8	0.6	9.7
ZrO_2	7.2	9.1	2.9	10.4	6.0	3.3	5.0	7.0	2.4	4.4	0.7
UO_2	18.5	12.2	2.6	14.1	10.1	8.4	2.7	12.7	5.7	1.3	2.0

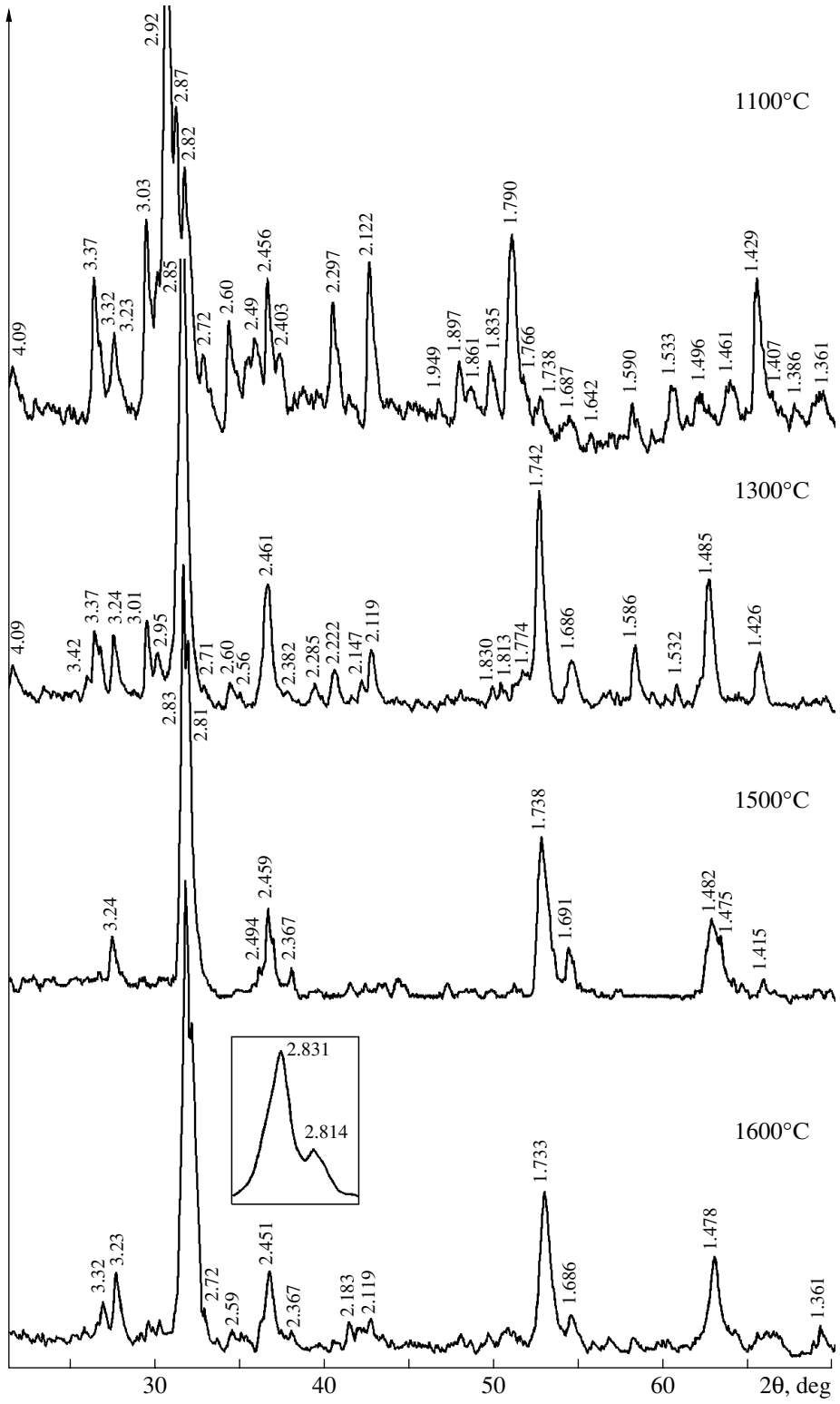

Fig. 12. X-ray patterns of samples produced from a charge of the same composition under different synthesis conditions. The inset demonstrates the structure of the main reflection of murataite in the ceramic produced with IMCC.

M8 and M3 in a proportion of about 1.5 : 1.0; rutile occurs in a subordinate amount (~10%), as does murataite M5 (~5%).

The structural relationships testify to the following crystallization sequence: M5, M8, M3, and rutile. The specific distribution of rutile grains as parallel linear

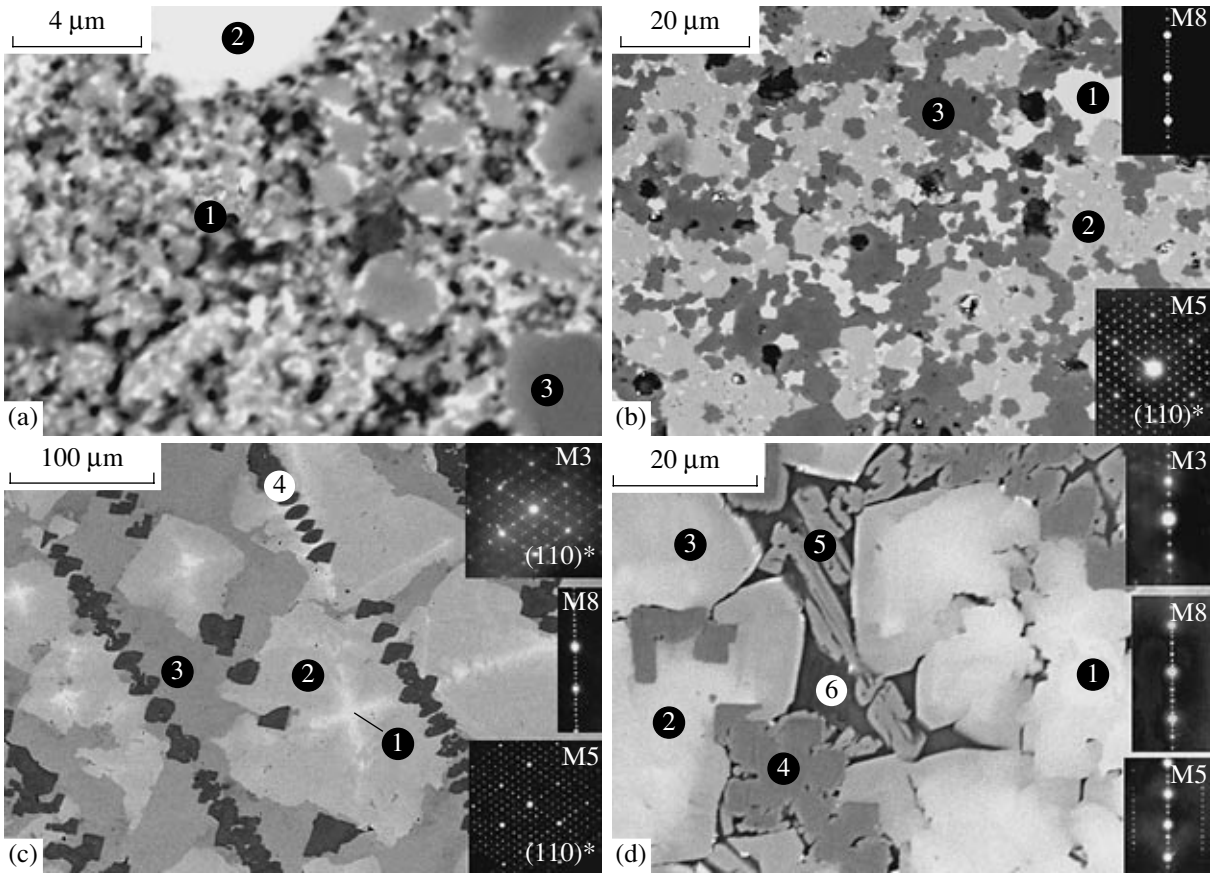

Fig. 13. SEM images of ceramics of the same composition produced under different conditions. The insets demonstrate microdiffraction patterns of murataite phases. (a) 1100°C: 1 is aggregate of murataite grains; 2, ZrO_2-based solid solution; and 3, rutile; (b) 1300°C: 1 is M5; 2, M8; and 3, rutile; (c) 1500°C: 1 is M5; 2, M8; 3, M3; and 4, rutile; (d) 1600°C, IMCC: 1 is M5; 2, M8; 3, M3; 4, rutile; 5, crichtonite; and 6, glass.

bands crosscutting all murataite varieties is notable and indicates that diffusion redistribution of Ti in the melt occurs rather rapidly and crystallization of rutile is controlled by energetically favorable conditions of crystal growth.

The ceramic obtained by IMCC is composed largely of murataite (75%, all varieties) and much smaller amounts of rutile (15%), crichtonite (5%), and glass (5%). According to the TEM and HRTEM data, murataite is represented by the M5, M8, and M3 structural varieties, which occur in the inner, intermediate, and outer zones of crystals, respectively (Figs. 12, 13). As in the ceramic obtained at 1500°C, the M5/M8 boundaries are diffuse, while the M8/M3 boundaries are more distinct. Rutile occurs as grains irregular in shape that fill interstices between murataite crystals. Tiny crichtonite grains replace rutile and make up oblong crystallites up to 5 μm in size incorporated into glass (Fig. 13). The compositions of crystalline phases are characterized by the same trends of element fractionation as in the ceramics produced with other methods (Table 8).

The observed phase relations show that the melt crystallization begins with formation of murataite M5, which further gives way to murataites M8 and M3. Rutile and crichtonite crystallize from the residual melt, and the process is completed with solidification of glass. The appearance of glass consisting of (wt %) 3.7 Na_2O, 16.1 Al_2O_3, 32.0 SiO_2, 18.4 CaO, 11.9 TiO_2, 10.6 MnO, and 2.1 Fe_2O_3 was caused by contamination of melt with material of the refractory coating of the crucible.

It should be emphasized that the difference in the structure of the ceramics produced by melting is related not so much to the temperature as to the specific features of synthesis in an electric furnace and by IMCC. In the latter case, the volume of the charge is much greater, the melt is formed under a temperature gradient, and crystallization proceeds under fast cooling. Furthermore, components of the coating enter the melt. The specific features of ceramics produced with the cold crucible technology indicate that a degree of fractionation of elements such as that taking place during melting in an electric furnace is not reached.

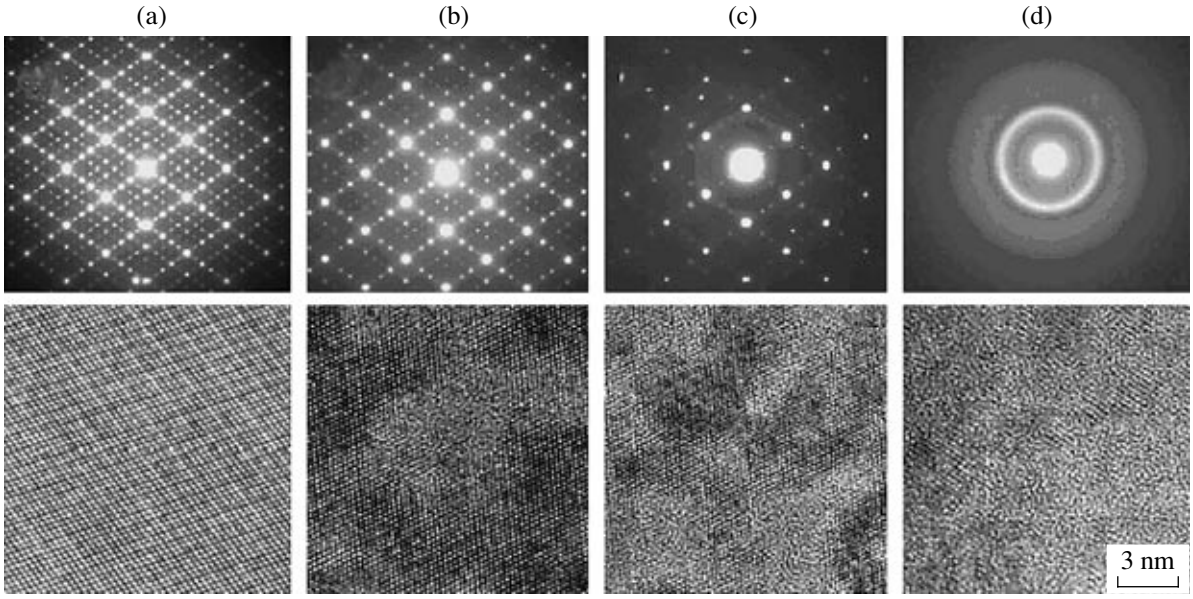

Fig. 14. Variation of the character of electron diffraction under ion beam irradiation of murataite M5 and the corresponding HRTEM images. (a) Before irradiation, (b) 4.38×10^{13} Kr^{2+}/cm^2 (0.04 displacements/atom), (c) 9.39×10^{13} Kr^{2+}/cm^2 (0.08 displacements/atom), (d) 15.6×10^{13} Kr^{2+}/cm^2 (0.13 displacements/atom).

In conclusion, it must be admitted that both the ceramics produced by cold compaction in combination with sintering at 1300°C and the melted ceramics possess the properties necessary for their use as a waste matrix. The choice of the industrial method of actinide immobilization in murataite ceramics will be determined primarily by its technological and economic efficiency.

THE RADIATION STABILITY OF MURATAITE

The estimation of radiation damage on the basis of mineral analogues cannot be used because radioactive elements are absent in natural murataite. Therefore, the radiation stability of synthetic murataites was studied after irradiation by an ion beam or by incorporation of the isotope ^{244}Cm (half-life 18 yr) into the crystal lattice.

Irradiation with Heavy Ions

Two samples of similar composition that consisted of several murataite varieties were chosen for irradiation with ions. The first sample was synthesized by melting in a platinum ampoule at 1500°C, and the second sample was produced by IMCC. The specific features of these samples were considered in the preceding section. Murataites M5 and M8 were studied in the first sample, and M3 and M5, in the second sample (Table 8).

The samples were irradiated with 1 MeV Kr^{2+} ions; the beam density was ~10^{12} ions/(cm^2 s). The encounter of heavy ions with target atoms well mimics the processes that occur on decay of actinides (Weber and Ewing, 2002). The experiments were performed on an ion accelerator at Argonne National Laboratory in the United States, and afterward the samples were studied with TEM at the University of Michigan (Lian et al., 2005).

The intensity of reflections in an electron diffraction pattern decreases with increasing irradiation dose, and the diffuse ring typical of an amorphous substance eventually appears instead of point diffraction. The consecutive steps of murataite lattice destruction with increasing irradiation dose are shown in Fig. 14. At 25°C, all murataite varieties are characterized by a dose of amorphization equal to 0.2 displacements/atom. This value is close to the dose of amorphization for most known HLW matrices, including pyrochlore- and zirconolite-based ones. According to calculations, a matrix that contains 10 wt % weapons ^{239}Pu, with a half-life of 24 ka, will accumulate a dose of irradiation equal to 0.2 displacements/atom over 500–700 yr. At an elevated temperature, amorphization requires higher doses of irradiation because heating promotes the return of atoms to their initial sites and recovery of the primary structure.

Ionic irradiation makes it possible to study the radiation damage to samples at both normal and elevated temperatures. The range from 100 to 250°C is the most important because these conditions are most probable for deep geological waste storage facilities. An exponential relationship between the amorphization dose and the temperature was established (Lian et al., 2005). The dose only slightly increases while the temperature rises to 400–500°C; then its growth becomes more appreciable. This is caused by recovery of radiation defects and return of atoms to their initial sites; heating promotes these processes. At an elevated temperature, in particular, at 600°C, the character of diffraction

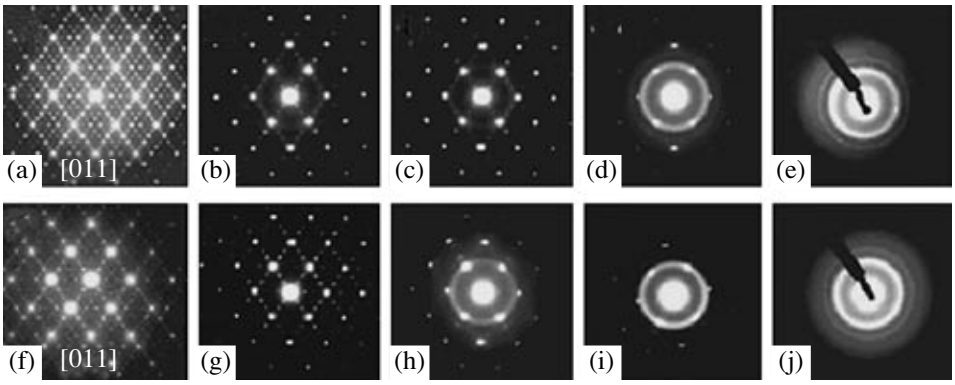

Fig. 15. Variation of diffraction of (a–e) murataite M5 and (f–j) M8 in the course of ion beam irradiation of sample 1 at 600°C. (a) Before irradiation, (b) 3.125×10^{14} Kr^{2+}/cm^2 (0.25 displacements/atom), (c) 5.625×10^{14} Kr^{2+}/cm^2 (0.45 displacements/atom), (d) 7.5×10^{14} Kr^{2+}/cm^2 (0.60 displacements/atom), (e) 13.75×10^{14} Kr^{2+}/cm^2 (1.1 displacements/atom), (f) before irradiation, (g) 1.875×10^{14} Kr^{2+}/cm^2 (0.15 displacements/atom), (h) 3.75×10^{14} Kr^{2+}/cm^2 (0.29 displacements/atom), (i) 7.5×10^{14} Kr^{2+}/cm^2 (0.58 displacements/atom), (j) 11.25×10^{14} Kr^{2+}/cm^2 (0.88 displacements/atom).

(Fig. 15) changes in the same way as at 25°C; however, the dose of irradiation that gives rise to amorphization is much higher in this case. Above a certain critical temperature, the rate of annealing of defects exceeds the rate of their appearance and the structure is retained unchanged at any dose of irradiation. In the studied samples, the critical temperature ranges from 650 to 750°C.

Radiation Effect of the Isotope ^{244}Cm on Murataite-Based Ceramics

Samples that contained curium isotopes were synthesized to study their radiation damage. This investigation was carried out together with specialists from RIAR. A charge of the composition (wt %) 11.7 CaO, 11.9 MnO, 60.5 TiO_2, 5.1 ZrO_2, 6.6 Fe_2O_3, and 4.2 Al_2O_3 was doped with ThO_2 and percolated with a nitrate Cm solution with an isotopic composition of 76% ^{244}Cm ($T_{1/2}$ = 18 yr) + 15% ^{245}Cm (8500 yr) + 9% ^{246}Cm (4730 yr). The bulk of the radiation dose is related to the decay of short-lived ^{244}Cm. The amount of curium provided a ^{244}Cm content equal to 1.8 wt %. As a result, a mixture of the composition (wt %) 10.5 CaO, 10.6 MnO, 8.1 ThO_2, 54.0 TiO_2, 4.6 ZrO_2, 6.0 Fe_2O_3, 3.8 Al_2O_3, and 2.4 Cm_2O_3 was obtained, with a specific radioactivity of 5.5×10^{10} Bq/g. This charge was pressed into pellets at room temperature and then sintered for 4 h at 1350°C in a platinum crucible. As a result, the pellets were melted with formation of a ceramic layer at the crucible bottom. According to the XRD data, the sample was murataite-based and contained traces of perovskite. Judging by the location of the main reflections in X-ray patterns, variety M5 prevailed over M8, which occurred in a lesser amount. The high radioactivity precluded microprobe analysis and the study of Cm distribution between the phases.

The dose of murataite irradiation was calculated on the basis of curium concentrations in the sample and the time of its exposure. The initial stage of murataite lattice destruction was recorded at a radiation dose of 1.3×10^{17} α decays/g. The damage is expressed in the displacement of reflections toward smaller angles, although the initial X-ray pattern as a whole is retained. After the accumulation of a dose of 1.2×10^{18} α decays/g, the weak murataite reflections disappear and the intensity of the main reflection (d = 2.84 Å) decreases and its width increases, indicating a significant degree of amorphization. The maximum dose of irradiation accumulated to date is 1.7×10^{18} α decays/g, but this dose did not give rise to amorphization. The perovskite reflections are retained unchanged, probably, owing to the lower Cm concentration in perovskite in comparison with that in murataite. It may be expected that the murataite lattice will be destroyed at a radiation dose above 2×10^{18} α decays/g. This value is comparable with the stability of pyrochlore and zirconolite doped with ^{238}Pu or ^{244}Cm (Weber et al., 1986; Matzke and van Geel, 1996; Volkov et al., 2004; Strachan et al., 2005). Their lattices become amorphous after $(2.5–4.8) \times 10^{18}$ α decays/g, which corresponds to 0.2–0.4 displacements/atom.

Chemical Stability of Murataite in Aqueous Solutions

Stability with respect to aqueous solutions is one of the requirements on actinide matrices. Experiments on the leaching of actinides from a murataite ceramic of basic composition containing 10 wt % ^{239}Pu and 0.1 wt % ^{241}Am were performed. The murataite varieties dominated in the ceramic, and crichtonite occurred as an admixture (Fig. 7). Plutonium concentrates in murataite, while its content in crichtonite is below the detection limit (tenths of weight percent). The experiments on leaching were carried out in accordance with the standard procedure of the MCC-1 (Materials Char-

Table 9. Leaching of actinides from murataite-based ceramic with water

Time from onset of run, days	Activity of solution, pulses/s		Concentration of element in solution, g/l		Rate of leaching, g/(m^2 day)	
	Pu	Am	Pu	Am	Pu	Am
3	1.830	0.154	2.22×10^{-5}	3.39×10^{-8}	8.37×10^{-3}	5.48×10^{-3}
7	0.345	0.147	4.25×10^{-6}	3.23×10^{-8}	6.88×10^{-4}	5.23×10^{-3}
14	0.584	0.142	7.19×10^{-6}	3.12×10^{-8}	5.82×10^{-4}	2.39×10^{-3}
21	0.198	0.131	2.40×10^{-6}	2.88×10^{-8}	1.30×10^{-4}	1.55×10^{-3}
28	0.039	0.0193	4.73×10^{-7}	4.25×10^{-9}	1.91×10^{-5}	2.34×10^{-4}
35	0.0537	0.0297	6.51×10^{-7}	6.53×10^{-9}	2.11×10^{-5}	2.88×10^{-4}
42	0.0499	0.0331	6.05×10^{-7}	7.28×10^{-9}	1.63×10^{-5}	2.68×10^{-4}
49	0.0640	0.0298	7.76×10^{-7}	6.60×10^{-9}	1.79×10^{-5}	2.08×10^{-4}
56	0.0411	0.0428	4.99×10^{-7}	9.42×10^{-9}	1.01×10^{-5}	1.90×10^{-4}
63	0.0547	0.0542	6.64×10^{-7}	1.19×10^{-8}	1.19×10^{-5}	2.14×10^{-4}

acterization Center) test. Samples and distilled water were loaded into Teflon containers, which were placed into a thermostat at $T = 90$°C. After standing for a given time, the containers were taken out to refresh the solution and then placed into the thermostat again. The first change of solution was performed after three days; the second, after four days; and further changes, weekly. The actinide contents in units of radioactivity were measured with an Alpha Analyst device and afterward recalculated into concentrations for clearness. Further, the rates of Pu and Am leaching from a sample were calculated from the equation

$$R_i = a_i/(A_i S t_n),$$

where a_i is the radioactivity (Bq) of the radionuclide or its mass (g) that passed into solution over a given span of time; A_i is the specific activity of the radionuclide (Bq/g) or its concentration (g/g) in the sample; S is the area of the sample surface (m^2); and t_n is the duration of the nth period of leaching, measured in days (*GOST* (State Standard) *R 52126-2003*, 2003). The rate decreases from 10^{-3} g/m^2 per day in the first days of the experiment to 10^{-4}–10^{-5} g/m^2 per day after 63 days of interaction (Table 9). The rate of americium leaching is several times higher than that of plutonium.

A similarly low rate of actinide leaching was established by a single-pass flow-through test of the powdered matrix. Two samples of the composition (wt %) 5 Al_2O_3, 10 CaO, 55 TiO_2, 10 MnO, 5 Fe_2O_3, 5 ZrO_2, and 10 AnO_2 (An = Th, U) were used for this purpose. The samples consisted of 90 vol % murataites M5, M8, and M3 and admixtures of crichtonite, pyrophanite, and perovskite (Figs. 6, 7; Table 3). The experiment was conducted at 90°C and a water flow rate of 1–3 ml/h; the total duration of the run was 33 days. The solution collected over a day was analyzed with ICP MS. The rates of U and Th leaching were calculated from the formula

$$R_i = (C_i q)/(f_i S),$$

where C_i is the concentration of the element (g/m^3) in the solution, q is the velocity of the water flow (m^3/day), f_i is the weight fraction of the element in the sample, and S is the area of the solid-phase surface (m^2). The rate of leaching over the whole time of interaction was ~10^{-6} g/(m^2 day).

Because several (commonly two or three) murataite varieties occur in a sample, it is impossible to estimate their stability separately. While the sample is interacting with water, the large alkali and alkali earth cations pass into solution most readily, whereas poorly soluble Ti, Zr, and Al accumulate at the sample surface. Hence, the stability of the matrix should increase with decreasing proportion of low- to high-charge cations in its composition. In murataite phases, the former are represented by Ca^{2+} and Mn^{2+} and the latter, by Ti^{4+}, Zr^{4+}, Al^{3+}, and Fe^{3+}. Thus, the phase stability in solutions will rise in the succession M5–M8–M3. Because murataite M3, which is depleted in radionuclides, commonly occurs in the outer zones of the zonal murataite grains in ceramics, this variety will hamper the removal of actinides from the matrix into solution and thus increase the corrosion stability of the matrix.

STRUCTURE OF SYNTHETIC MURATAITES: A MODERN CONCEPT

The interpretation of the structure of synthetic murataite and the confirmation of its crystallochemical formula are unsolved problems that are of key importance for understanding isomorphic replacements in the matrices, actinides and REE included. The data on natural murataite cannot be used in full measure because of a substantial difference in chemical composition. Furthermore, as was mentioned above, natural murataite is characterized by a structure with a threefold parameter of the fluorite-type unit cell. Among the synthetic phases are not only such a variety but also

murataites with other repetition factors of the structure, and the phases with five- and eightfold repetition are prevalent in actinide matrices.

The occurrence of perovskite and crichtonite in the sample was confirmed by the XRD study of a murataite ceramic with the Rietveld method using the international XRD data set. Despite the fact that the X-ray attributes of natural murataite are presented in this data set under number 86-0888, the reflections of synthetic murataites are referred to oxide [$(Fe_{0.88}Ti_{1.11}Zr_{0.94})O_5$] with fluorite structure (space group *Fm3m*, $Z = 1$), a = 4.9274 Å. As can be seen, this result conflicts with the data on the real phase composition of the sample, where murataite phases with 5- and 8-fold unit cells are predominant (Fig. 3). The cause of this discrepancy is different position of reflections from planes with the same indices in X-ray patterns of natural and synthetic murataites. In particular, the d spacing of the main reflection (hkl = 333) for the mineral equals 2.86 Å, whereas the d values of the main reflections for synthetic varieties (333 for M3, 555 for M5, and 888 for M8) range from 2.79 to 2.86 Å.

The study of murataites with TEM and HRTEM allowed internal periodicity of the structure, with combination of atomic rows into groups consisting of two and three layers (M5) or three and five layers (M8), to be revealed (Karimova et al., 2002). Proceeding from this periodicity, it was suggested that synthetic murataites are made up of blocks or modules that represent two cognate structures: pyrochlore with a double fluorite cell and murataite with a triple cell (Urusov et al., 2005). In terms of this hypothesis, the structure of murataite M5 has one pyrochlore-type and one murataite M3 layer, while murataite M8 has one pyrochlore-type and two murataite M3 layers. At the same time, murataite M7 has one murataite and two pyrochlore-type modules. Taking into account these relationships, the generalized formulas of synthetic murataites have been calculated. For pyrochlore and murataite M3, these formulas are [$R_2M_2O_7$] and [$R_3M(1)_6M(2)_2O_{20}$], respectively, where R sites are occupied by Ca, Mn, REE, and actinide; M(1) sites, with Ti and Zr; and M(2) sites, with Fe, Al, and Ga. In this case, formula M5 appears as [$R_5M(1)_8M(2)_2O_{27}$]; formula M8, as [$R_8M(1)_{14}M(2)_4O_{47}$]; and formula M7, as [$R_7M(1)_{10}M(2)_2O_{34}$] in accordance with the differences detected in their compositions. As follows from this model, the contents of actinides, Zr, and REE diminish in the series pyrochlore > M7 > M5 > M8 > M3, while the Ti, Al, and Fe contents increase in the same direction.

This model also accounts for the difference in d spacings for murataite varieties, which is the most obvious when all the varieties occur in the same sample. Depending on the composition, the d value of the main reflection increases from 2.79–2.82 Å for murataite M3 to 2.82–2.85 Å for M8 and 2.84–2.86 Å for M5. A maximum d value of 2.86–2.87 Å is typical of M7. A still higher value d = 2.89–2.95 Å is established for the main reflection (222) of the REE–actinide titanates, which should be regarded in terms of this hypothesis as an end member of the murataite–pyrochlore series. It is noteworthy that murataite M7 occurs in multicomponent ceramics very rarely but is common in the HREE–Mn–Ti–O system, where HREE are heavy REE from Gd to Lu or Y (Kir'yanova et al., 2002).

CONCLUSIONS

We have worked out a new crystalline matrix for actinide wastes based on artificial murataite, which is close in structure to the rare natural mineral of the same name that is a Na, Ca, HREE, Zn, and Nb titanate with a structure derived from the fluorite lattice. However, synthetic murataite contains actinides, Mn, and Zr instead of Na, Zn, and Nb. To study the properties of synthetic murataite, we synthesized samples of REE-, actinide-, REE–actinide-, and Ga-bearing murataite-based matrices.

Murataite-based ceramics characterized by complete phase formation can be synthesized by cold compaction combined with subsequent sintering at 1300°C for 4 h or by melting at 1500–1600°C with the subsequent crystallization of the melt.

In contrast to the natural murataite, with a triple motif of fluorite type, among the synthetic phases, varieties with three- (M3), five- (M5), seven- (M7), and eightfold (M8) repetition of the basic fluorite cell were established.

The compositional and structural variations of synthetic murataites with a lattice repetition factor of >3 are explained by participation of murataite M3 and pyrochlore blocks in their structure.

The highest murataite content in the samples reaches 95 vol %. Despite the variation of charge compositions and synthesis conditions, we failed to produce a purely murataite matrix. Other titanate phases—crichtonite, rutile, Fe–Mn-titanate with ilmenite–pyrophanite structure, perovskite, and pyrochlore—always occur in addition to murataite.

The murataite grains in melted ceramics are commonly zonal, with cores composed of M5 (occasionally M7), intermediate zones with a prevalence of M8, and outer zones that consist of M3. The actinide, Zr, and REE contents in the series M5 (M7)–M8–M3 drop by several times, while the Ti, Al, and Fe contents increase in the same direction. The zoning creates an additional protective barrier because the core enriched in actinides is surrounded by a shell with lower concentrations that prevents the actinides and related elements from passing into solution.

In chemical and radiation stability, murataite is comparable with other titanate ceramics or surpasses the latter. Yet it is a more universal matrix that includes not only actinides, Zr, and REE, but also other elements

of HLW, especially products of corrosion (Mn, Fe, Al, Ga, etc.).

Various types of wastes can be incorporated into a murataite-based matrix: the actinide–Zr–REE fraction of liquid HLW, Am–Ga remains of plutonium conversion into MOX fuel, particular actinides, and other actinide-bearing HLW that contain REE and corrosion products. Up to 350 kg of elements derived from HLW can be incorporated into 1 t of such a ceramic.

ACKNOWLEDGMENTS

We thank O.I. Stefanovskaya (Kir'yanova), A.G. Ptashkin, and N.S. Mikhailenko for their assistance in synthesis of samples; L.A. Kochetkova, M.I. Lapina, A.V. Mokhov, and A.V. Sivtsov for cooperation in their study; S.A. Perevalov and G.A. Varlakova for carrying out the experiments on leaching; A.N. Lukinykh as well as R. Ewing, and J. Lian both from the University of Michigan for carrying out radiation tests; and T. Hartmann from the University of Nevada for the study of murataites with the Rietveld method. This work was supported by the Russian Foundation for Basic Research (project no. 05-05-08000) and by the Federal Agency for Science and Innovations (state contract no. 02.434.11.4007).

REFERENCES

1. J. W. Adams, T. Botinelly, W. N. Sharp, and K. Robinson, "Murataite, a New Complex Oxide from El Paso County, Colorado," Am. Mineral. **59** (1/2), 172–176 (1974).
2. *End Points for Spent Nuclear Fuel and High-Level Radioactive Waste in Russia and the United States* (National Academies Press, Washington DC, 2003).
3. T. S. Ercit and F. C. Hawthorne, "Murataite, a UB_{12} Derivative Structure with Condensed Keggin Molecules," Can. Mineral. **33**, 1223–1229 (1995).
4. *GOST* (State Standard) *R 50926-96. Solidified High-Level Radioactive Waste. General Technical Requirements* (Gosstandart Rossii, Moscow, 1996) [in Russian].
5. *GOST* (State Standard) *R 52126-2003. Radioactive Waste. Testing of the Chemical Stability of Solidified High-Level Radioactive Waste by Long-Term Leaching* (Gosstandart Rossii, Moscow, 2003) [in Russian].
6. O. V. Karimova, N. I. Organova, and V. G. Balakirev, "Modulation in the Murataite Structure," Kristallografiya **47** (6), 1027–1030 (2002) [Crystallography Reports **47** (6), 957–960 (2002)].
7. O. I. Kir'yanova, S. V. Stefanovsky, S. V. Yudintsev, and B. S. Nikonov, "The Effect of CaO : Gd_2O_3 and CaO : UO_2 Ratios on the Phase Composition of Ceramics in the CaO–Gd_2O_3 (UO_2)–MnO–TiO_2 System," Perspektivnye Materialy, No. 5, 38–45 (2002).
8. A. A. Kopyrin, A. I. Karelin, and V. A. Karelin, *Technology of Production and Radiochemical Reprocessing of Nuclear Fuel* (Atomenergoizdat, Moscow, 2006) [in Russian].
9. N. P. Laverov, A. I. Gorshkov, S. V. Yudintsev, et al., "New Structural Variations of Synthetic Murataite," Dokl. Akad. Nauk **363** (4), 540–543 (1998a) [Dokl. Earth Sci. **363A** (9), 1272–1274 (1998a)].
10. N. P. Laverov, B. I. Omel'yanenko, S. V. Yudintsev, and B. S. Nikonov, "Zirconolite As a Matrix for Immobilization of High-Level Radioactive Waste," Geol. Rudn. Mestorozhd. **38** (5), 387–395 (1996) [Geol. Ore Deposits **38** (5), 345–352 (1996)].
11. N. P. Laverov, B. I. Omel'yanenko, S. V. Yudintsev, et al., "Mineralogy and Geochemistry of Matrices for the Immobilization of High-Level Radioactive Waste," Geol. Rudn. Mestorozhd. **39** (3), 211–228 (1997) [Geol. Ore Deposits **39** (3), 179–193 (1997)].
12. N. P. Laverov, B. I. Omel'yanenko, S. V. Yudintsev, and B. S. Nikonov, "Objectives of Mineralogical Studies in Connection with Radioactive Waste Disposal," in *Proceedings of Conference on Ecological Mineralogy* (IGEM, Moscow, 1998b), pp. 5–36 [in Russian].
13. N. P. Laverov, I. A. Sobolev, S. V. Stefanovsky, et al., "Synthetic Murataite: A New Mineral for Actinide Immobilization," Dokl. Akad. Nauk **362** (5), 670–672 (1998c) [Dokl. Earth Sci. **363** (8), 1104–1106 (1998c)].
14. N. P. Laverov, S. V. Yudintsev, B. I. Omel'yanenko, et al., "Murataite Ceramics for the Immobilization of Actinides," Geol. Rudn. Mestorozhd. **41** (2), 99–108 (1999) [Geol. Ore Deposits **41** (2), 85–93 (1999)].
15. N. P. Laverov, S. V. Yudintsev, S. V. Stefanovsky, and Ya. N. Dzhang, "New Actinide Matrix with Pyrochlore Structure," Dokl. Akad. Nauk **381** (3), 399–402 (2001) [Dokl. Earth Sci. **381A** (9), 1053–1056 (2001)].
16. N. P. Laverov, S. V. Yudintsev, S. V. Stefanovsky, et al., "Phase Formation during the Synthesis of Actinide Matrices," Dokl. Akad. Nauk **383** (1), 95–98 (2002) [Dokl. Earth Sci. **383** (2), 190–193 (2002)].
17. N. P. Laverov, S. V. Yudintsev, T. S. Yudintseva, et al., "Effect of Radioactive Decay on Properties of Confinement Matrices of Actinide-Bearing Waste," Geol. Rudn. Mestorozhd. **45** (6), 483–513 (2003) [Geol. Ore Deposits **45** (6), 423–451 (2003)].
18. J. Lian, L. M. Wang, R. C. Ewing, et al., "Ion Beam-Induced Amorphization and Order-Disorder Transitions in the Murataite Structure," J. Applied Physics **97** (113536), (2005).
19. K. Maslakov, A. Teterin, Yu. Teterin, et al., "X-ray Photoelectron Spectroscopy Study of Plutonium-Containing Murataite-Based Ceramics," in *Proceedinds of the 36th Journées des Actinides Symposium: Abstract P-22* (Oxford, 2006).
20. Hj. Matzke and J. van Geel, "Incorporation of Pu and Other Actinides in Borosilicate Glass and Waste Ceramics," in *Disposal of Weapon Plutonium* (Kluwer Acad. Publ., 1996), pp. 93–105.
21. P. E. D. Morgan and F. J. Ryerson, "A New "Cubic" Crystal Compound," J. Mater. Sci. Lett. **1** (8), 351–352 (1982).
22. A. M. Portnov, L. S. Dubakina, and G. K. Krivokoneva, "Murataite in the Predicted Association with Landauite," Dokl. Akad. Nauk SSSR **261** (3), 741–744 (1981).
23. A. E. Ringwood, "Disposal of High-Level Nuclear Waste: A Geological Perspective," Mineral. Mag. **49**, 159–176 (1985).

24. S. V. Stefanovsky, O. I. Kir'yanova, S. V. Yudintsev, et al., "Phase Composition and Distribution of Elements in Murataite Ceramics Containing REE and Actinoids," Fiz. Khim. Obrab. Mater., No. 3, 72–80 (2001).
25. S. V. Stefanovsky, B. S. Nikonov, B. I. Omel'yanenko, et al., "Synthetic Molten Zirconolite-Based Materials for Immobilization of Radioactive Waste," Fiz. Khim. Obrab. Mater., No. 6, 111–117 (1997).
26. S. V. Stefanovsky, S. V. Yudintsev, and O. I. Kir'yanova, "The Effect of Synthesis Conditions on the Phase Composition of Pyrochlore–Brannerite Ceramics," Fiz. Khim. Obrab. Mater., No. 5, 90–98 (2001).
27. S. V. Stefanovsky, S. V. Yudintsev, B. S. Nikonov, and B. I. Omel'yanenko, "A Study of SYNROC Material," Geoekology, No. 4, 58–74 (1996).
28. S. V. Stefanovsky, S. V. Yudintsev, B. S. Nikonov, and O. I. Stefanovskaya, "Phase Composition of Ceramics in Systems with Rare Earth Elements, Manganese, and Titanium Oxides," Radiokhimiya **48** (2006) [Radiochemistry **48** (2006)] (in press).
29. D. M. Strachan, R. D. Scheele, E. C. Buck, et al., "Radiation Damage Effects in Candidate Titanates for Pu Disposition: Pyrochlore," J. Nucl. Mater, No. 345, 109–135 (2005).
30. V. S. Urusov, N. I. Organova, O. V. Karimova, et al., "Synthetic "Murataites" As Modular Members of the Pyrochlore–Murataite Polisomatic Series," Dokl. Akad. Nauk **401** (2), 226–232 (2005) [Dokl. Earth Sci. **401** (2), 319–325 (2005)].
31. V. S. Urusov, V. S. Rusakov, and S. V. Yudintsev, "Valence State and Structural Position of Fe Atoms in Synthetic Murataite," Dokl. Akad. Nauk **384** (4), 527–532 (2002) [Dokl. Earth Sci. **384** (4), 461–465 (2002)].
32. E. R. Vance, B. D. Begg, R. A. Day, and C. J. Ball, "Zirconolite-Rich Ceramics for Actinide Waste," in *Proceedings of Symposium on Scientific Basis for Nuclear Waste Management XVIII* (MRS, Pittsburgh, 1995), Vol. 353, pp. 767–774.
33. Yu. F. Volkov, S. V. Tomilin, A. N. Lukinykh, et al., "Titanate Ceramics with Pyrochlore Structure As a Matrix for Immobilization of Excess Weapons-Grade Plutonium," Radiokhimiya **46** (4), 322–328 (2004) [Radiochemistry **46** (4), 351–357 (2004)].
34. W. J. Weber and R. C. Ewing, "Radiation Effects in Crystalline Oxide Host Phases for the Immobilization of Actinides," in *Proceedings of Symposium on Scientific Basis for Nuclear Waste Management XXV* (MRS, Warrendale, 2002), Vol. 713, pp. 443–454.
35. W. J. Weber, J. W. Wald, and Hj. Matzke, "Effects of Self-Radiation Damage in Cm-Doped $Gd_2Ti_2O_7$ and $CaZrTi_2O_7$," J. Nucl. Mater. **138**, 196–209 (1986).
36. S. V. Yudintsev, "A Structural–Chemical Approach to Selecting Crystalline Matrices for Actinide Immobilization," Geol. Rudn. Mestorozhd. **45** (2), 172–187 (2003) [Geol. Ore Deposits **45** (2), 151–165 (2003)].
37. S. V. Yudintsev, S. V. Stefanovsky, B. S. Nikonov, and B. I. Omelianenko, "Phase and Chemical Stability of Murataite Containing Uranium, Plutonium and Rare Earth's," in *Proceeding of Symposium on Scientific Basis for Nuclear Waste Management XXIV* (MRS, Warrendale, 2001), Vol. 663, 357–366.